Journal of Virology

The Human T-Lymphotropic Virus Type 1 Tax Protein Inhibits Nonsense-Mediated mRNA Decay by Interacting with INT6/EIF3E and UPF1

Vincent Mocquet, Julia Neusiedler, Francesca Rende, David Cluet, Jean-Philippe Robin, Jean-Michel Terme, Madeleine Duc Dodon, Jürgen Wittmann, Christelle Morris, Hervé Le Hir, Vincenzo Ciminale and Pierre Jalinot

J. Virol. **2012, 86(14):7530. DOI: 10.1128/JVI.07021-11.**
Published Ahead of Print 2 May 2012.

JVI Journals ASM.org

The Human T-Lymphotropic Virus Type 1 Tax Protein Inhibits Nonsense-Mediated mRNA Decay by Interacting with INT6/EIF3E and UPF1

Vincent Mocquet,[a] Julia Neusiedler,[a]* Francesca Rende,[b] David Cluet,[a] Jean-Philippe Robin,[a] Jean-Michel Terme,[a]* Madeleine Duc Dodon,[a] Jürgen Wittmann,[c] Christelle Morris,[a] Hervé Le Hir,[d] Vincenzo Ciminale,[b] and Pierre Jalinot[a]

Laboratoire de Biologie Moléculaire de la Cellule, Unité Mixte de Recherche 5239, Centre National de la Recherche Scientifique, Ecole Normale Supérieure de Lyon, Lyon, France[a]; Department of Oncology and Surgical Sciences, Institute of Neuroscience at the Department of Biomedical Sciences, Università di Padova, Padua, Italy[b]; Division of Molecular Immunology, Department of Internal Medicine III, Nikolaus Fiebiger Center, University of Erlangen-Nürnberg, Erlangen, Germany[c]; and Institut de Biologie de l'Ecole Normale Supérieure, Unité Mixte de Recherche 8197, Centre National de la Recherche Scientifique UMR8197, Paris, France[d]

In this report, we analyzed whether the degradation of mRNAs by the nonsense-mediated mRNA decay (NMD) pathway was affected in human T-lymphotropic virus type 1 (HTLV-1)-infected cells. This pathway was indeed strongly inhibited in C91PL, HUT102, and MT2 cells, and such an effect was also observed by the sole expression of the Tax protein in Jurkat and HeLa cells. In line with this activity, Tax binds INT6/EIF3E (here called INT6), which is a subunit of the translation initiation factor eukaryotic initiation factor 3 (eIF3) required for efficient NMD, as well as the NMD core factor upstream frameshift protein 1 (UPF1). It was also observed that Tax expression alters the morphology of processing bodies (P-bodies), the cytoplasmic structures which concentrate RNA degradation factors. The presence of UPF1 in these subcellular compartments was increased by Tax, whereas that of INT6 was decreased. In line with these effects, the level of the phosphorylated form of UPF1 was increased in the presence of Tax. Analysis of several mutants of the viral protein showed that the interaction with INT6 is necessary for NMD inhibition. The alteration of mRNA stability was observed to affect viral transcripts, such as that coding for the HTLV-1 basic leucine zipper factor (HBZ), and also several cellular mRNAs sensitive to the NMD pathway. Our data indicate that the effect of Tax on viral and cellular gene expression is not restricted to transcriptional control but can also involve posttranscriptional regulation.

Human T-lymphotropic virus type 1 (HTLV-1) infection is associated with the onset of severe diseases, mainly adult T-cell leukemia (ATL) and tropical spastic paraparesis, also named HTLV-1-associated myelopathy, in 2 to 5% of patients (for a review, see reference 44). These conditions are characterized by a long latency, with infection often occurring in childhood and disease development at an adult age. Accordingly, it is estimated that the development of ATL involves several phases, ending in the acute proliferation of monoclonal ATL cells. At the initial stage, lymphocytes are infected by viral particles, leading to provirus integration and the expression of various viral proteins. Among them, Tax plays an important role both by inducing the transcription of the provirus and by stimulating the proliferation of the host cell. Tax, which is present in both the nucleus and the cytoplasm, exerts these functions by directly binding or by modulating the expression of several key cellular proteins involved in transcriptional control, cell cycle progression, genomic stability, cell adherence and migration, protein degradation, and RNA metabolism (7).

Among these various cellular proteins bound by Tax, we have previously characterized INT6, also known as EIF3E, one the 13 subunits of the translation initiation factor eukaryotic initiation factor 3 (eIF3) (16). The complex between both proteins was found to be cytoplasmic, whereas in normal cells, INT6 is present in both the cytoplasm and the nucleus (16, 27, 64). In mammalian cells, the silencing of INT6 seems to marginally affect general translation, but evidence for a role of INT6 in the translation of specific genes was recently obtained (26, 67). Regarding its role in association with eIF3, we have previously shown that INT6 was important for the degradation of cellular mRNAs by nonsense-mediated mRNA decay (NMD) (47). The latter is a quality control process leading to the degradation of mRNAs, including a premature stop codon (PTC), which can arise from mutation or aberrant alternative splicing and eventually prevents the synthesis of a truncated protein, which could serve as a dominant negative protein against an intact protein (3). NMD also regulates the expression of mRNA with upstream open reading frame (ORF) (uORF) or long 3′-untranslated (3′UTR) sequences. After a first round of translation (12, 30), the presence of a PTC more than 50 nucleotides upstream of an exon-exon junction leads to the association of the SMG1-eRF1-eRF3-UPF1 complex (SURF) with the mRNA. Upstream frameshift protein 1 (UPF1) then interacts with the UPF2 and UPF3 proteins present in the nearby exon junction complex (EJC) (11, 33). These interactions lead to the phosphorylation of UPF1 by SMG1 and the routing of the mRNA toward degradation (31), which presumably occurs in cytoplasmic compartments known as processing bodies (P-bodies) (49, 57). P-bodies are cytoplasmic foci that contain proteins involved in different aspects

Received 7 December 2011 Accepted 20 April 2012
Published ahead of print 2 May 2012
Address correspondence to Pierre Jalinot, pjalinot@ens-lyon.fr.
* Present address: Julia Neusiedler, Wellcome Trust Centre for Gene Regulation and Expression, University of Dundee, Dundee, United Kingdom; Jean-Michel Terme, Molecular Biology Institute of Barcelona (IBMB), CSIC, Barcelona, Spain.
V.M. and J.N. equally contributed to this work.
Supplemental material for this article may be found at http://jvi.asm.org/.

doi:10.1128/JVI.07021-11

of mRNA turnover, such as the decapping enzyme DCP1 and the XRN1 exonuclease, also including NMD factors (14, 53). Concomitantly with degradation, UPF1, which is also present in P-bodies, is dephosphorylated by SMG5 and PP2A and can then be recycled to bind novel mRNAs (51).

It was shown previously that the deregulation of gene expression in stressed cells was due in part to the modification of mRNA stability (20). Moreover, while previous works associated the presence of a PTC in tumor suppressor genes (such as WT1, p53, and BRCA1) with the development of cancers (19, 34, 36, 52), recent data demonstrated that NMD inhibition plays an important role in the initiation of tumorigenesis (1, 5, 18, 28, 52, 63) and the potential expression of truncated tumor suppressor factors (3). By considering the multifactorial process of leukemogenesis in HTLV-1 cells, the role of INT6 in the NMD pathway, and the effect of Tax on INT6, we asked whether Tax was able to modulate the NMD process. By using functional assays, we observed that this mRNA surveillance pathway was effectively downregulated in Tax-expressing cells. In line with this activity, Tax binds both INT6 and UPF1 and inhibits interactions between these two NMD factors. In agreement with these abilities, Tax expression alters the morphology of P-bodies and stabilizes cellular and viral RNAs prone to NMD degradation by acting at the posttranscriptional level.

MATERIALS AND METHODS

Constructs, cell culture, and transfection. The following plasmids used in NMD assays were previously described: globin NS39 (GlNS39) and wild-type (WT) globin (GlWT) (47) and wild-type and mutated β-globin fused to *Renilla* luciferase (6). The HTLV-1 basic leucine zipper factor (HBZ), expression vector was generated from the *HBZ* ORF including the 3′ long terminal repeat (LTR) of plasmid pCSHTLV-I (15) by using oligonucleotides A and B. In parallel, the pUC 19 backbone from pCSHTLV-I was amplified by using primers C and D. After digestion by EcoRV and EcoRI, both the vector and insert were ligated, creating pCS-HBZ. Sequences of the primers are as follows: 5′-AACTTGATATCGCCTCTCCAGCGCCCG-3′ for primer A, 5′-AACTTGAATTCCACTTGGCCGTGGGCCAAG-3′ for primer B, 5′-AACTTGAATTCACTGGCCGTCGTTTTACAACGTCG-3′ for primer C, and 5′-AACTTGATATCAAGCTTGGCGTAATCATGGTCATAGC-3′ for primer D.

All T-cell lines (Jurkat, JPX9, TL-OmI, C91PL, HUT102, and MT2) were transfected by using Fugene 6 (Promega). For JPX9 cells, Tax expression was induced by the addition of 150 μM $ZnCl_2$ for various times. The cell culture medium was changed, and 24 h later, reporter constructs were transfected. 293T cells were transfected by a calcium phosphate procedure described previously (62). In the case of DNA and small interfering RNA (siRNA) cotransfection, 293T cells were first transfected with the siRNAs by using Lipofectamine 2000 (Invitrogen) reagent according to the manufacturer's instructions. After 24 h, the medium was changed, and the transfection of DNA vectors was done by the calcium phosphate procedure. For viral mRNA analysis, 48 h after the transfection of siRNAs with Lipofectamine 2000, cells were transfected with 2 μg of the HTLV-1 molecular clone pACH by using GeneJuice reagent (Novagen) for 20 to 24 h.

NMD assays and qRT-PCR. NMD assays with HeLa cells with the GlNS39 and GlWT constructs were performed as described previously (47), and mRNAs were measured by quantitative reverse transcription-PCR (qRT-PCR) using the QuantiTect SYBR green qRT-PCR kit (Qiagen) and β-globin primers. Similarly, for the analysis of *GADD45*α, *SLIT2*, *BAG1*, *ATF4*, and *MAP3K14* mRNA half-lives, total RNA was extracted by using the Nucleospin RNA kit (Macherey-Nagel). One-step qRT-PCR (QuantiTect SYBR green qRT-PCR kit) was further performed by using appropriate primers with normalization with respect to glyceraldehyde-3-phosphate dehydrogenase (GAPDH) mRNA (47).

In T cells, 2 μg of the WT or NS39 globin-*Renilla* luciferase construct was transfected together with 1 μg of firefly luciferase reporter plasmid, which was used for normalization. The NMD assay was carried out according to a dual-luciferase assay procedure reported previously (6). mRNAs were measured by qRT-PCR using the QuantiTect SYBR green qRT-PCR kit (Qiagen) and appropriate primers, as previously described (47). The values presented in the graphs correspond to the means of data from at least three independent measures, with error bars corresponding to standard deviations. The asterisks in the figures correspond to the results of Student's *t* test (two tailed and unpaired).

For the analysis of HTLV-1 RNA primer/probe sequences, cycling profiles and absolute quantitations of transcripts were carried out as previously described (54). The $\Delta\Delta C_T$ method was applied to verify the silencing of *UPF1*. The data presented are the means of data from six independent measurements. For *HBZ* mRNA analysis, 8 μg of pCS-HBZ and 1 μg of a *Renilla* luciferase expression vector plasmid were transfected into HeLa cells with Lipofectamine 2000 together with or without pSG-Tax (1 μg). The *HBZ sp1* mRNA was reverse transcribed by using the High Capacity cDNA reverse transcription kit (Roche Applied Science) by using primer 5′-AACTGTCTAGTATAGCCATCA-3′ and then PCR amplified with the following oligonucleotides: 5′-GCCGATCACGATGCGTTTCCC-3′ and 5′-GGCAGAACGCGACTCAACCG-3′.

Protein production, purification, and GST pulldown. Glutathione *S*-transferase (GST), GST-Tax, His-GST-INT6, and His-UPF1 were produced in BL21 Codon+ *Escherichia coli* cells. INT6 was produced and purified according to a protocol reported previously (60). The His-GST tag was removed after proteolysis overnight by use of a His-GST-tobacco etch virus (TEV) protease while dialyzing the eluted INT6 with buffer (50 mM NaH_2PO_4 [pH 8], 300 mM NaCl, 1 mM dithiothreitol [DTT], 5% glycerol), followed by an additional purification on Ni-nitrilotriacetic acid (NTA) resin. His-UPF1 was produced as previously reported (11). GST and GST-Tax proteins were produced as previously described (9). Briefly, bacteria were induced with isopropyl-β-D-thiogalactopyranoside (IPTG) at 28°C for 3 h. The bacteria were then resuspended in MTBS (150 mM NaCl, 12.5 mM Na_2HPO_4, 2.5 mM KH_2PO_4, 100 mM EDTA [pH 7.3], 10% glycerol), lysed by sonication (4 times for 30 s), and centrifuged at 10,000 rpm for 1 h. The lysate was incubated with glutathione-agarose beads in the presence of 1% Triton X-100. The beads were washed in DE80 buffer (20 mM Tris [pH 7.9], 5% glycerol, 80 mM KC1, 1 mM $MgC1_2$, 0.2 mM EDTA, 10 μM $ZnCl_2$, 0.5 mM DTT, 0.5 mM phenylmethylsulfonyl fluoride [PMSF]) plus 1% Triton X-100 and either eluted with elution buffer (20 mM reduced glutathione, 20 mM Tris-HCl [pH 7.9]) or incubated with purified UPF1 (11) or purified INT6 (60) in DE80 buffer plus 0.1% Triton and 5 mg/ml bovine serum albumin (BSA). After 3 washes, proteins were eluted from the beads and analyzed by immunoblotting.

Immunofluorescence. A total of 0.05×10^6 HeLa cells were transfected by the calcium phosphate procedure. Cells were fixed for 20 min with fresh 4% paraformaldehyde, washed 3 times, and incubated with phosphate-buffered saline (PBS)–1% BSA. Cells were incubated with the primary antibody for 1.5 h at room temperature, washed 3 times, and further incubated for 1 h with the secondary antibody. Finally, cells were mounted in 10 μl of Vectashield 4′,6-diamidino-2-phenylindole (DAPI) (1.5 μg/ml) (Vector Laboratories). Slides were observed with an LSM 510 confocal microscope (Zeiss). For quantification, fluorescence intensity was analyzed by using the ImageJ program (National Institutes of Health).

Immunoprecipitation. Immunoprecipitations were conducted as described previously (62), using the following antibodies: rabbit antisera to INT6 (C-20, N-19, or C-169, as indicated in the figures) (46, 48); rabbit polyclonal antibodies to UPF1 and UPF2 (65); mouse monoclonal antibody to phospho-UPF1, which was kindly provided by A. Yamashita (clone 8E6) (66); rabbit polyclonal antibody to phospho-Ser/Thr ATM/ATR substrate (catalog number 2851; Cell Signaling Technology); mouse monoclonal antibody to Tax (clone 474); and mouse monoclonal antibodies to the FLAG (clone M2; Sigma) and hemagglutinin (HA) (clone 7; Sigma) epitopes.

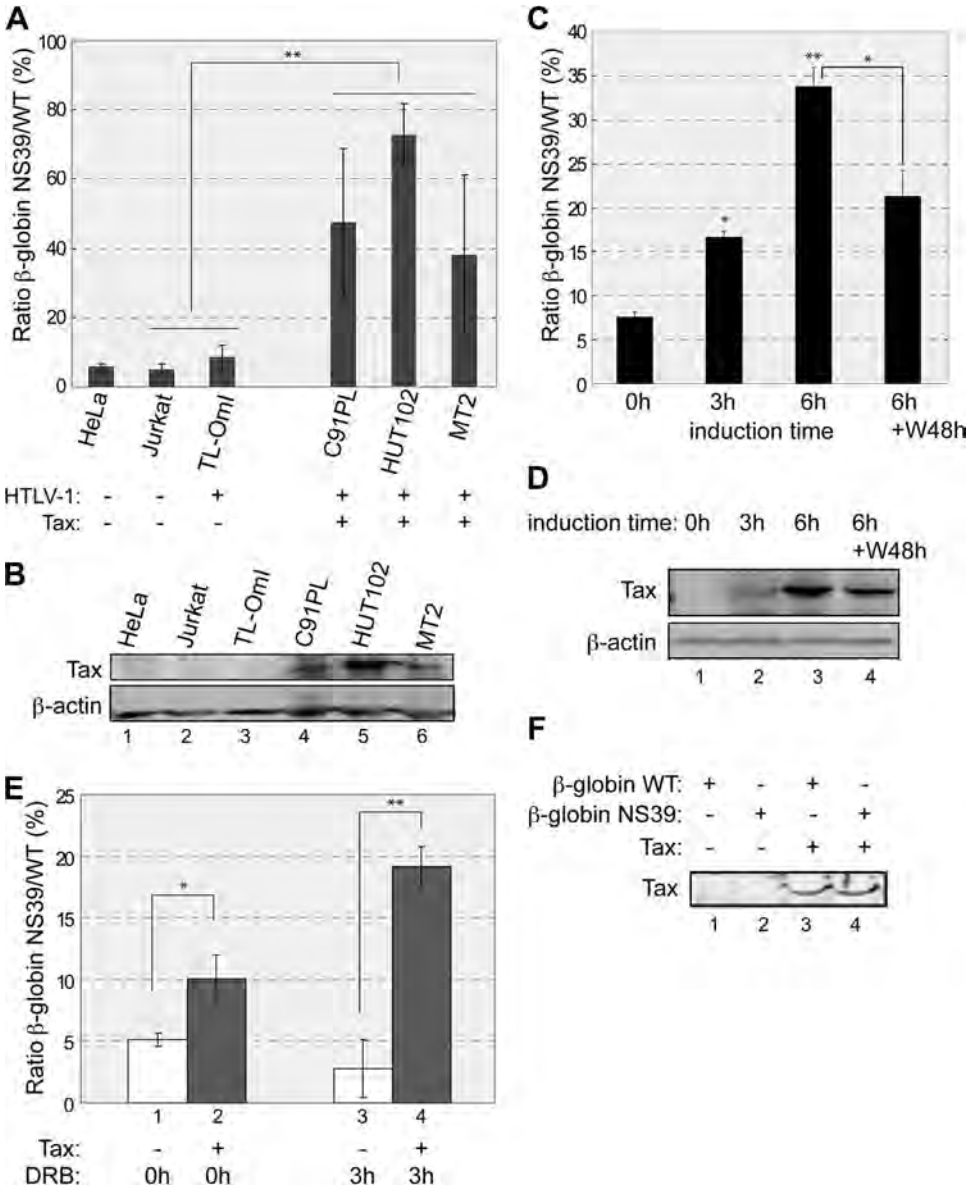

FIG 1 Effect of Tax on stability of NMD-prone mRNA. (A) NMD assays were performed with the indicated cell lines. The *Renilla* luciferase activity from the GlNS39 plasmid was normalized and expressed as a percentage of that from the GlWT plasmid. The bar graph represents mean values, with error bars corresponding to standard deviations. The Student *t* test corresponds to Tax-expressing cell lines versus non-Tax-expressing cell lines, as indicated (**, $P < 0.01$). (B) Extracts from panel A were analyzed by immunoblotting with antibodies to Tax (top) and to β-actin (bottom). (C) NMD assays were performed with JPX9 cells without (0 h) or with Tax induction for 3 h or 6 h. The 6 h+W48h bar corresponds to cells washed and further cultured for 48 h after 6 h of induction (*, $P < 0.05$; **, $P < 0.01$ [Student's *t* test results refer to the 0-h conditions, except for 6 h+W48 {6 h of induction}]). (D) Extracts used in panel C were analyzed by immunoblotting with antibodies to Tax and to β-actin. (E) NMD assays were performed with HeLa cells in the absence (lanes 1 and 3) or in the presence (lanes 2 and 4) of Tax expression, without (lanes 1 and 2) or with (lanes 3 and 4) the addition of 100 μg/ml DRB for 3 h. The percentage of GlNS39 mRNA with respect to GlWT mRNA is represented as described above for panel A. (F) Extracts used in panel E were analyzed by immunoblotting with an antibody to Tax.

RESULTS

HTLV-1 Tax inhibits mRNA degradation via the NMD pathway. We first evaluated whether the NMD pathway is downregulated in HTLV-1-infected cells. This evaluation was carried out by performing NMD assays using reporter plasmids including either wild-type β-globin (GlWT) or a PTC at position 39 (GlNS39) fused to the *Renilla* luciferase coding sequence (6). Control or HTLV-1-infected cell lines (HeLa, Jurkat, TL-OmI, C91PL, HUT102, and MT2 cells) were transfected with these reporter plasmids, and the levels of luciferase activities corresponding to wild-type and NS39-mutated β-globin sequences were quantified. As expected, in the HeLa and Jurkat cell lines, the GlNS39-associated activity represented only a small percentage of the activity associated with wild-type β-globin (Fig. 1A). In contrast, in the cell lines expressing the complete provirus with an active 5′ LTR (C91PL, HUT102, and MT2), the levels of GlNS39-associated activity were increased and much closer to that corresponding to wild-type β-globin (Fig. 1A). The strongest effect was observed on

HUT102 cells, which express a higher amount of Tax than do C91PL and MT2 cells (Fig. 1B, compare lane 5 to lanes 4 and 6). Interestingly, in the TL-OmI cells, which include the HTLV-1 sequence but which do not express Tax (Fig. 1B, lane 3), the NMD activity evaluated by this assay was very similar to that observed for the control HeLa and Jurkat cell lines. These results suggested that the NMD activity is downregulated in HTLV-1-expressing cells and that Tax was possibly involved in this effect.

To address the role of Tax more directly, we carried out assays with JPX9 cells, which are Jurkat cell derivatives expressing Tax under the control of a metallothionein promoter which can be induced by the addition of Zn^{2+} cations in the culture medium (61). Depending on the duration of induction, we observed increasing Tax expression levels (Fig. 1D), which correlated with a significant increase in the level of activity of the GlNS39 reporter, with the ratio with respect to the wild type increasing from 7% in the absence of Tax to 34% at 6 h postinduction (Fig. 1C). We also carried out a reversal of Tax induction by washing the cells after a 6-h induction and culturing them for 48 h in the absence of Zn^{2+} cations. Under these conditions, the intracellular concentration of Tax decreased (Fig. 1D, compare lanes 3 and 4), and this correlated with a significant drop of the GlNS39/GlWT ratio from 34% to 21% (Fig. 1C). We also analyzed the decay of the mRNAs after a transcription blockade by the addition of the RNA polymerase II (Pol II) elongation inhibitor 5,6-dichloro-1-β-D-ribofuranosylbenzimidazole (DRB). In agreement with the luciferase activity measurements, a specific stabilization of the mRNA including the NS39 mutation in the presence of Tax was observed (see Fig. S1A in the supplemental material).

This NMD inhibition was also analyzed with HeLa cells, which were transfected with vectors expressing wild-type and NS39-mutated β-globin mRNAs without fusion to the *Renilla* luciferase coding sequence, and both mRNAs were quantified by qRT-PCR. According to previously reported observations (43), in the absence of Tax coexpression, the amount of GlNS39 mRNA was only 5% of that of GlWT (Fig. 1E, lane 1). In the presence of Tax, we observed a 2-fold increase in the GlNS39/GlWT ratio (Fig. 1E, lane 2, and F, lane 3). Moreover, when analyzed 3 h after the addition of DRB, this GlNS39/GlWT ratio dropped from 5% to 2.5% in the absence of Tax (Fig. 1E, lane 3), while this ratio increased from 10% to 18% in the presence of the viral protein (Fig. 1E, compare lanes 2 and 4, and see Fig. S1B in the supplemental material). This indicated a specific posttranscriptional effect of Tax on GlNS39 mRNA stability. Collectively, these observations indicated that Tax is able to stabilize an NMD-sensitive transcript.

Tax binding to INT6 and to the UPF1-UPF2 complex. We then analyzed the association of Tax with the NMD core factors. First, an immunoprecipitation directed against Tax in HUT102 cells was performed, and the presence of UPF1, UPF2, and INT6 was checked by immunoblotting. Jurkat cell extracts were used as a control. The intracellular concentrations of UPF1, UPF2, and INT6 were similar in both extracts (Fig. 2A, lanes 1 and 2). We found that Tax associates with these 3 factors in the HTLV-1-infected cell line HUT102 (Fig. 2A, lanes 3 and 4). Similar immunoprecipitations were done with antibodies to UPF1, UPF2, or INT6 by using RNase A-treated extracts from C8166 cells (see Fig. S2A in the supplemental material), and a Tax signal was detected specifically after immunoprecipitation with all three antibodies (see Fig. S2B, lane 1, in the supplemental material). In order to determine whether these interactions were direct, recombinant, highly purified INT6, GST-Tax, and His-UPF1 were produced (see Fig. S2C in the supplemental material). GST pulldown assays showed that Tax is able to interact with UPF1 as well as INT6 (Fig. 2B and C, lane 1). In contrast, purified INT6 and UPF1 were unable to interact directly together (Fig. 2D), in agreement with our previously reported observations indicating that the INT6-UPF1 interaction was dependent on RNA (47).

We further analyzed this network of interactions and how the presence of Tax affects the composition of the NMD complex. To this end, 293T cells were transfected with different combinations of vectors expressing Tax, INT6-FLAG, HA-UPF1, and HA-UPF2. Immunoprecipitations were carried out by using and antibody to the HA epitope, and immunoprecipitated proteins were analyzed by immunoblotting with antibodies to the HA epitope,

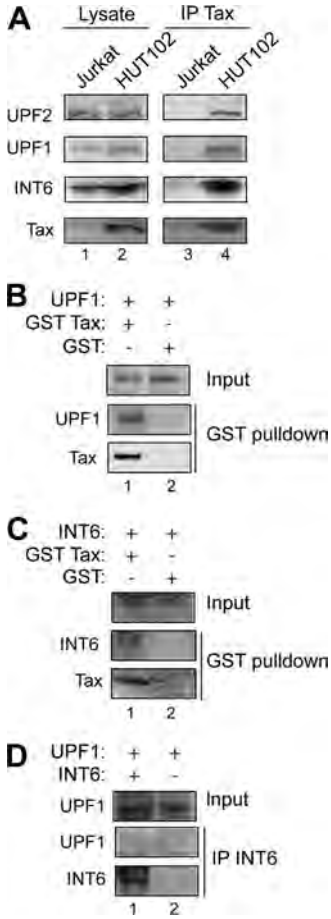

FIG 2 Interaction of Tax with NMD factors. (A) Extracts of Jurkat (lane 1) and HUT102 (lane 2) cells treated with RNase A were analyzed by immunoblotting with antibodies to UPF2, UPF1, INT6, and Tax. Using these Jurkat (lane 3) and HUT102 (lane 4) cell extracts, immunoprecipitation (IP) with an antibody to Tax was carried out, and the immunoprecipitates were analyzed by immunoblotting with the same set of antibodies. (B) GST, GST-Tax, and UPF1 were produced in bacteria and purified. UPF1 was mixed with GST-Tax (lane 1) or GST (lane 2), and a GST pulldown was carried out. The presence of UPF1 (middle) and Tax (bottom) in the eluates was assessed by immunoblotting. The top panel corresponds to 2% of the input. (C) Same as B, with purified INT6 instead of UPF1. (D) Purified INT6 and UPF1 were mixed, and immunoprecipitation was carried out with the N-19 antibody to INT6 (lane 1). The immunoprecipitate was analyzed by immunoblotting with antibodies to UPF1 (middle) and to INT6 (bottom). As a control, the same experiment was done in the absence of purified INT6 (lane 2).

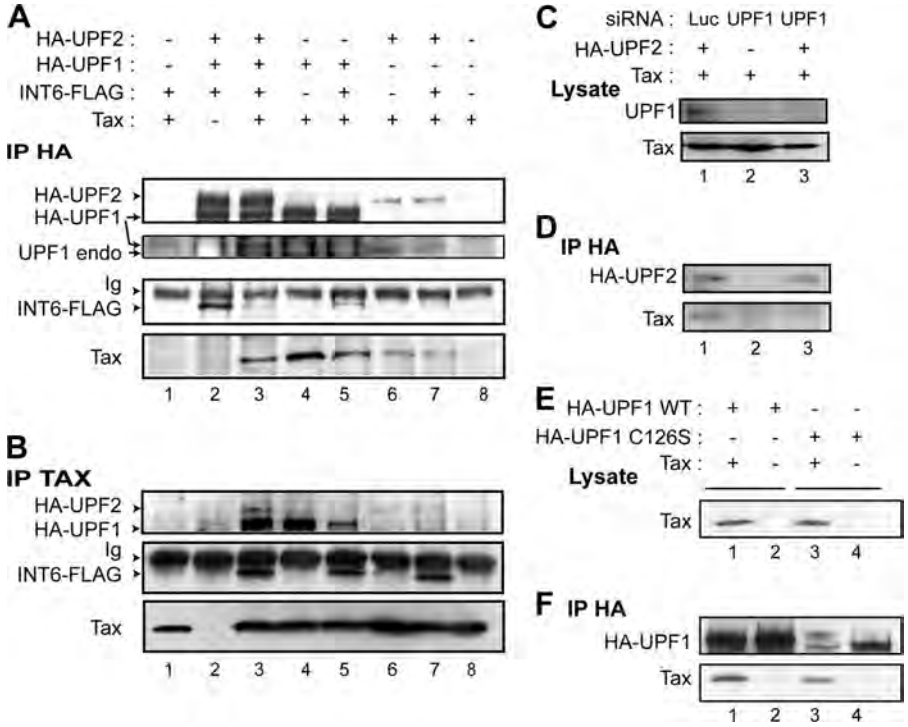

FIG 3 Network of interactions between Tax, INT6, UPF1, and UPF2. (A) Extracts of 293T cells transfected with Tax, INT6-FLAG, HA-UPF1, and HA-UPF2 expression vectors, as indicated, were used for immunoprecipitations using the antibody to the HA epitope. Immunoprecipitates were analyzed by immunoblotting using antibodies to HA (top), UPF1 (top middle), FLAG (bottom middle), and Tax (bottom). Ig marks the signal of the immunoglobulin heavy chain. (B) The same extracts were also immunoprecipitated with an antibody to Tax, and immunoprecipitates were analyzed by immunoblotting with antibodies to HA (top), FLAG (middle), and Tax (bottom). (C) 293T cells were transfected with either control (luciferase) (lane 1) or anti-UPF1 (lanes 2 and 3) siRNA duplexes as well as with vectors expressing Tax (lanes 1 to 3) and HA-UPF2 (lanes 1 and 3). Protein levels of endogenous UPF1 (top) and Tax (bottom) were monitored by immunoblotting. (D) Extracts of these transfected cells were used for immunoprecipitations carried out with the antibody to HA, and immunoprecipitates were analyzed by immunoblotting with antibodies to HA (top) and to Tax (bottom). (E) 293T cells were transfected with vectors expressing HA-UPF1, either the wild type (lanes 1 and 2) or including the C126S mutation (lanes 3 and 4) and Tax (lanes 1 and 3). Tax expression in the cell extracts was monitored by immunoblotting. (F) Extracts of these transfected cells were used for immunoprecipitations using the antibody to HA, and coimmunoprecipitated proteins were analyzed by immunoblotting with antibodies to HA (top) and to Tax (bottom).

UPF1, the FLAG epitope, and Tax (Fig. 3A). In agreement with data from the experiments described above, the immunoprecipitations of both UPF1 and UPF2 led to a clear Tax signal (Fig. 3A, bottom, lane 3). Similar results were obtained when HA-UPF1 and HA-UPF2 were transfected and immunoprecipitated separately (Fig. 3A, lanes 4 and 6, respectively); however, in the latter case, the HA-UPF2 and Tax signals were markedly weaker. This is likely due to a stabilizing effect of UPF1 on UPF2 expression under these conditions. By precipitating Tax, we confirmed its association with HA-UPF1, HA-UPF2, and INT6-FLAG (Fig. 3B, lanes 1, 3, 4, and 6). As a control for the specificity of Tax binding to these factors, we checked that Tax does not bind to coexpressed FLAG-green fluorescent protein (GFP) under these conditions (see Fig. S3B and S3C in the supplemental material). In these experiments, the association of Tax with HA-UPF2 was possibly mediated by endogenous UPF1. In this regard, a weak endogenous UPF1 signal was detected after the immunoprecipitation of HA-UPF2 alone (Fig. 3A, top middle, lanes 6 and 7). In order to clarify this point, we silenced UPF1 by RNA interference while transiently expressing Tax and HA-UPF2 (Fig. 3C). The level of Tax associated with HA-UPF2 was then reduced to a background level (Fig. 3D, bottom, compare lanes 1 and 3), indicating that UPF1 is likely to bridge Tax and UPF2. In this regard, by using the UPF1 C126S mutant, a mutant that does not bind UPF2 (33), it was observed that the binding of Tax to UPF1 was independent of its association with UPF2 (Fig. 3E and F). Collectively, these experiments confirmed that Tax associates with INT6 (16) and showed the binding of Tax to the core NMD complex through an interaction with UPF1.

Displacement of INT6 from UPF1 by Tax binding. In the same experiment, it was also observed that Tax expression decreased the amount of INT6 immunoprecipitated by UPF1 and UPF2, suggesting that Tax prevents the association of INT6 with these NMD factors (Fig. 3A, bottom middle, compare lanes 2 and 3). This observation was not related to a weaker expression of FLAG-INT6 (see Fig. S3A in the supplemental material). Similarly, while a clear association of Tax with HA-UPF1 was observed after the immunoprecipitation of HA-UPF1 or Tax, this level of binding was decreased when INT6 was coexpressed (Fig. 3A and B, compare lanes 4 and 5). These data suggested that Tax binds INT6, forming a complex that cannot associate with the upstream frameshifts (UPFs). We confirmed this with endogenous NMD proteins in HeLa cells, where INT6 coimmunoprecipitated much less endogenous UPF1 in the presence of Tax (compare lanes 1 and 2 in Fig. S3E, top, in the supplemental material). These observations support the notion that Tax competes for the binding of INT6 to an NMD complex including UPF1. This point was also addressed by performing confocal microscopy analyses to observe

the subcellular localizations of these proteins. We observed that in the absence of Tax, approximately 80% of the rare HA-UPF1 cytoplasmic foci were also stained by the antibody to INT6, while in the presence of Tax, no more than 20% of UPF1 spots colocalized with INT6 (see Fig. S4A and S4B in the supplemental material). These combined results led us to conclude that Tax, by interacting with both UPF1 and INT6, impairs their association.

Tax leads to the accumulation of UPF1 in P-bodies. In order to better understand the effect of Tax binding on the functioning of UPF1, we further analyzed how Tax modifies the subcellular localization of UPF1. It was previously reported that UPF1 is partially localized in P-bodies and that the inhibition of mRNA degradation increases this localization (57). For these analyses, HeLa cells were transfected with vectors expressing HA-UPF1, DCP1-red fluorescent protein (RFP) (a component of the P-bodies), and either a control or a Tax expression vector (Fig. 4A). In the absence of Tax, and in agreement with previous reports, DCP1 fluorescence was observed mainly in a limited number (3 to 9) of small cytoplasmic foci corresponding to the P-bodies (35) (Fig. 4Ac). UPF1 was homogeneously distributed in the cytoplasm, with rare small foci which often colocalized with DCP1 (Fig. 4Ab, and see Fig. S4C in the supplemental material). In the presence of Tax, numerous and larger cytoplasmic foci of UPF1 appeared (Fig. 4Ag). This point was confirmed by quantifying the number of UPF1 foci and the UPF1 fluorescence present in three cellular compartments (the cytoplasm, cytoplasmic foci, and nucleus). This analysis confirmed the increase in the number of UPF1 foci and showed that the presence of Tax leads to a significant decrease in the diffuse cytoplasmic staining of UPF1 (−17%) to the benefit of cytoplasmic foci (10-fold increase) (Fig. 4B and C). Similarly, the DCP1 foci were much larger than those in the absence of Tax (compare Fig. 4Ac and h, and see Fig. S4C, S5A, and S5B in the supplemental material). UPF1 and DCP1 still colocalized in the presence of Tax (Fig. 4Ai and j, and see Fig. S4C in the supplemental material). We were also able to identify other known components of the P-bodies, Ago2 and p54, in these DCP1 cytoplasmic foci, suggesting that Tax increases the storage of UPF1 in P-bodies and causes their enlargement (Fig. 4D, and see Fig. S5A in the supplemental material). In the absence of Tax, INT6 similarly showed discrete cytoplasmic foci that colocalized with those corresponding to DCP1 fluorescence, which is in agreement with a role of INT6 in NMD (see Fig. S6 in the supplemental material). In the presence of Tax, the sizes of the INT6 foci did not increase as for UPF1 and marginally colocalized with the enlarged P-bodies (see Fig. S4A, S4B, and S6 in the supplemental material). In agreement with the notion that Tax causes a disruption of UPF1/INT6 binding, these observations clearly show that the viral protein affects the subcellular localizations of INT6 and UPF1 differently. In order to correlate the accumulation of UPF1 in P-bodies with its interaction with Tax, we first looked at the localization of the viral protein in cells expressing DCP1-RFP and p54-GFP. In the absence of Tax, DCP1 and p54 displayed the usual pattern for P-bodies, while Tax led to the formation of DCP1 and p54 cytoplasmic foci with unusual sizes and numbers (Fig. 4Db, c, g, and h, and see Fig. S4C in the supplemental material). This effect was dependent on the amount of Tax (data not shown). Moreover, we were able to identify a colocalization of Tax with these unusual P-bodies (Fig. 4D). In addition, in HA-UPF1-transfected cells, we observed an increased presence of Tax in the cytoplasm and several foci exhibiting Tax, UPF1, and DCP1 costaining (Fig. 4A). These observations are in agreement with the interaction of Tax with UPF1 during RNA processing and suggest that Tax might play a direct role in the alteration of the P-bodies.

In P-bodies, UPF1 is dephosphorylated by the phosphatase PP2A, which is recruited via the SMG5-SMG7 complex (51) and then leaves the P-bodies to possibly reenter a novel round of RNA processing (17). Accordingly, we further tested whether the accumulation of UPF1 in P-bodies was linked to an alteration of this dephosphorylation step. To address this point, cells were transfected with the HA-UPF1 vector together with either a control or a Tax expression vector (Fig. 5A). Extracts were analyzed with an antibody raised against phosphorylated UPF1 (66) and another one which recognizes the S/TQ motifs phosphorylated by phosphatidylinositol 3-kinase kinases (PI3KKs) such as SMG1, the NMD UPF1 kinase. The expression of Tax increased the intensity of the signal detected with both antibodies (Fig. 5A, middle and bottom, compare lanes 1 and 2), while the total amount of HA-UPF1 was unchanged (Fig. 5A, top). A densitometric analysis of the blot showed a >2-fold increase in the phosphorylated form after normalization to the total amount of UPF1. An immunoprecipitation of Tax was also performed with these extracts and revealed that Tax associates with phosphorylated UPF1 (Fig. 5B, middle and bottom). We further analyzed the association of these phosphorylated forms of UPF1 with SMG5, which is part of the NMD dephosphorylation complex. Cells were transfected with different combinations of Tax, HA-SMG5, and UPF1 (without the HA tag) expression plasmids. Immunoprecipitations were carried out against the HA tag of SMG5, and the presence of UPF1 in the immunoprecipitates was analyzed by immunoblotting. In the absence of Tax, UPF1-SMG5 complexes could not be detected, presumably due to UPF1 dephosphorylation in the presence of overexpressed SMG5 (Fig. 5C and D, lane 1). In the presence of Tax and with similar levels of immunoprecipitated HA-SMG5, UPF1 was clearly detected (Fig. 5D, lane 2). Collectively, these data suggest that Tax is able to inhibit NMD-dependent UPF1 dephosphorylation, leading to the stabilization of the SMG5-UPF1 association.

Inhibition of NMD by Tax depends on its interaction with INT6. In order to better understand how Tax inhibits NMD, we tested the effects of three different Tax mutants: Tax M22, which is inactive for NF-κB activation (58); Tax M47, which is inefficient in transactivating CREB-responsive promoters (32); and Tax K1-10R, in which all lysines potentially modified by ubiquitination were mutated to arginines. The latter mutant is defective with respect to both the NF-κB and CREB pathways (13, 50). The effects of these Tax mutants were assessed by using the NMD assay. In agreement with the results shown in Fig. 1A, the level of expression of wild-type Tax in HeLa cells increased the GlNS39/GlWT ratio to approximately 9%. The expression of Tax M22 and Tax K1-10R led to a stronger increase (20% and 18%, respectively). In contrast, with the Tax M47 mutant, the GlNS39/GlWT ratio was unchanged with respect to that observed in the absence of Tax, indicating a complete lack of activity of this mutant (Fig. 6A). We further tested whether this inactivity was due to a protein-protein interaction defect. Cells were transfected with vectors expressing HA-UPF1 and INT6-FLAG together with a control plasmid or the different Tax expression vectors (Fig. 6B to D). Tax immunoprecipitations were carried out, and the presence of HA-UPF1 and INT6-FLAG in the immunoprecipitates was analyzed by immunoblotting. Interestingly, the binding of M47 to HA-UPF1 was slightly increased (1.5-fold), but the interaction with INT6-FLAG

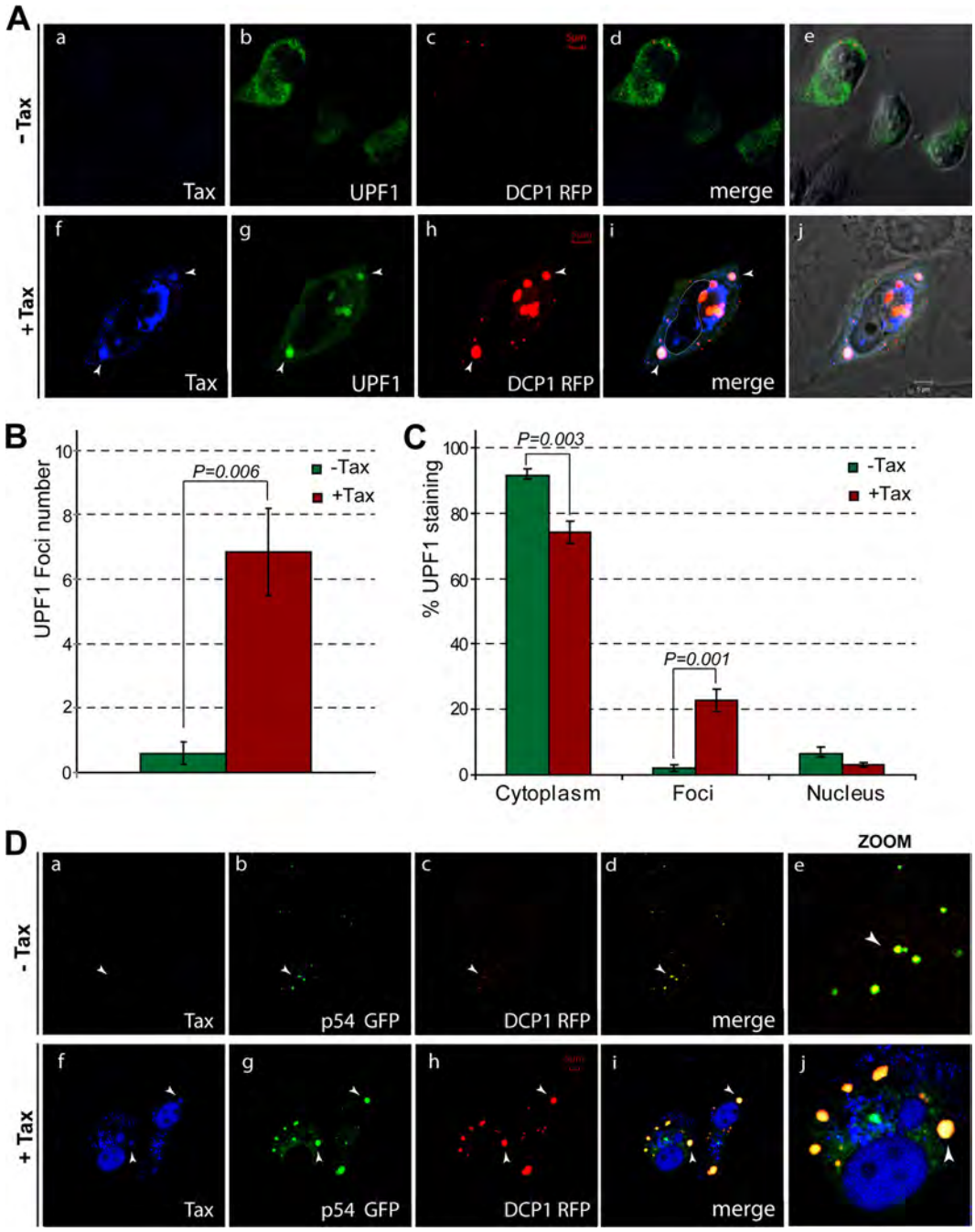

FIG 4 Colocalization of Tax and NMD factors with P-bodies. (A) Confocal microscopy analysis of HeLa cells transfected with HA-UPF1 and DCP1-RFP expression vectors together with a control (a to e) or Tax (f to j) expression vector. Immunostaining was done with antibodies to Tax (blue) (a and f) and to HA (green) (b and g). The DCP1-RFP fluorescence was also analyzed (red) (c and h). Panels d and i correspond to the superposition of the three fluorescences, with the nucleus limits identified from the transmission view, highlighted with a white line. Panels e and j correspond to the superposition of all three fluorescences with the transmission view. (B) Quantification of the UPF1 foci observed in the absence or presence of Tax. The numbers of UPF1 foci in several cells ($n = 10$) were determined, and the mean number of foci under both conditions is represented (green, without Tax; red, with Tax), with error bars corresponding to standard deviations. The statistical significance of the difference between both conditions was calculated with Welch's *t* test and is indicated on the graph. (C) Similarly to panel B, the UPF1 fluorescence in the cytoplasm outside the foci, in the cytoplasmic foci, and in the nucleus in the absence or the presence of Tax was quantified and is represented in a bar graph. (D) Confocal microscopy analysis of HeLa cells transfected with vectors coding for the P-body components p54-GFP and DCP1-RFP without or with 0.1 μg of the Tax-expressing plasmid. Immunostaining of Tax appears in blue (a and f), along with p54-GFP fluorescence (green) (b and g) and DCP1-RFP fluorescence (red) (c and h). Panels d and i correspond to a superposition of the three fluorescences, and panels e and j correspond to an enlargement of this image.

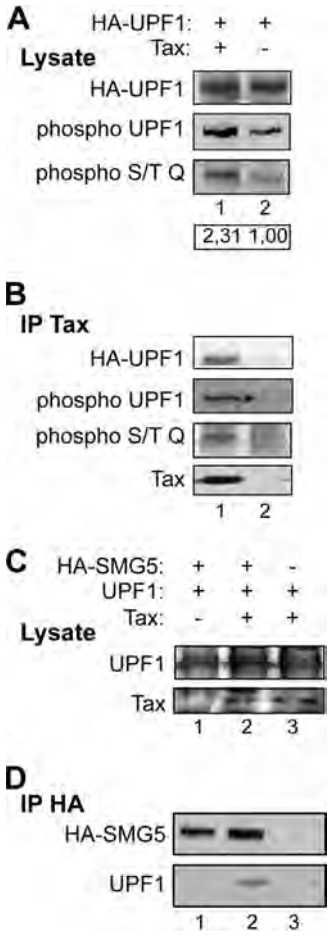

FIG 5 Tax stabilizes the phosphorylated forms of UPF1. (A) 293T cells were transfected with Tax and HA-UPF1 expression vectors, as indicated. Cell extracts were analyzed by immunoblotting with an antibody to HA (top), phosphorylated UPF1 (middle), or phosphorylated S/TQ motifs (bottom). The signals of phosphorylated UPF1 were quantified by densitometric analysis and normalized to those corresponding to total UPF1. The ratios of phosphorylated UPF1/total UPF1 are indicated below the blot images. (B) Extracts from panel A were immunoprecipitated with an antibody to Tax, and immunoprecipitates were analyzed by immunoblotting with the indicated antibodies. (C) 293T cells were transfected with HA-SMG5, UPF1, and Tax expression vectors, as indicated. Cell extracts were analyzed by immunoblotting using antibodies to UPF1 (top) and to Tax (bottom). (D) Extracts from panel C were immunoprecipitated with the antibody to HA, and immunoprecipitates were analyzed with antibodies to HA (top) and to UPF1 (bottom).

was markedly reduced (4-fold less) (Fig. 6D). In this experiment, equal quantities of Tax protein were precipitated (Fig. 6C). This observation indicates that Tax residues L319 and L320 are necessary for the association with INT6. We also observed that Tax M22 and Tax K1-10R bound more strongly to both INT6-FLAG (2-fold) and HA-UPF1 (3-fold) than did WT Tax. In these cases, it seems likely that the stronger interactions with INT6 and UPF1 resulted from an increased availability of Tax due to its loss of interactions with other partners, in particular those belonging to the NF-κB pathway. Hence, the interaction with INT6 appears to be essential for the inhibitory effect of Tax on NMD: Tax M22 and K1-10R, which bind INT6 more efficiently than the wild type, are more active in inhibiting the NMD, whereas Tax M47, which interacts poorly with this protein, is inactive. In induced JPX9 cells, it was also observed by performing an NMD assay that the overexpression of INT6 caused a significant decrease (39%) in the inhibition of NMD, likely due to Tax titration (see Fig. S7 in the supplemental material). A similar effect was observed with the overexpression of UPF1 (see Fig. S7 in the supplemental material).

We also analyzed the effects of the M22 and M47 Tax mutants on the P-body aspect. As expected, Tax M22 was able to increase the number and size of DCP1-RFP foci similarly to WT Tax (in both cases, approximately 80% of the cells exhibited abnormal P-bodies), while only a limited number of unusual DCP1-RFP foci were observed with Tax M47 (11% of the cells) (Fig. 6E). These data show a correlation between the abilities of Tax to functionally inhibit NMD and to modify the aspect of P-bodies. Moreover, a comparative analysis of P-body profiles and interaction efficiencies with the M47 mutant suggested that the Tax-INT6 association is a prerequisite for P-body deformation by UPF1 sequestration.

HTLV-1 mRNAs are sensitive to NMD. The identification of NMD inhibition in HTLV-1-expressing cells raised the question of the sensitivity of the various viral mRNAs to this process. To address this question, we transfected plasmid pACH, which includes the entire HTLV-1 provirus, into cells that were previously treated with either control or UPF1 siRNAs. Twenty-four hours after provirus transfection, RNAs were prepared from these cells and analyzed by qRT-PCR (54). Under these conditions, the level of UPF1 mRNA was reduced to approximately 20% of its level in control cells, indicating effective silencing (Fig. 7A). Although the sensitivities of the viral mRNAs to UPF1 silencing were variable, a significant increase was seen for all of them (Fig. 7B). This analysis suggested that viral RNAs are prone to UPF1-mediated degradation. Since we previously demonstrated that Tax was an important player in HTLV-1-associated NMD inhibition, we further tested whether it can stabilize such viral RNAs. To do so, we analyzed the *HBZ* transcript, which was selected because its transcription is much less sensitive to Tax than the other sense transcripts (V. Mocquet, unpublished data). *HBZ* mRNA is produced by the transcription of the antisense strand from the 3′ LTR and is expressed with or without alternative splicing. Here, HeLa cells were transfected with a provirus similar to the ACH used in Fig. 7B but lacking its 5′ LTR as well as the first 4 kb of coding sequence. Thus, this plasmid expresses *HBZ* mRNAs only under the control of the 3′ LTR. The alternatively spliced isoform of HBZ (sp1) is the main expressed isoform in ATL cells (10). Hence, we analyzed by qRT-PCR the decay of *HBZ sp1* mRNA, after the addition of DRB, in the presence or absence of Tax. This experiment showed that Tax increases the half-life of the *HBZ sp1* mRNA 2.6 times (Fig. 7C). Collectively, these data support the notion that Tax enhances the amount of some viral mRNAs by also acting at the posttranscriptional level through the inhibition of the NMD pathway.

Stability of NMD-prone cellular mRNA is modified in the presence of Tax. By testing a series of NMD-prone mRNAs, we previously observed that INT6 was required for the degradation of a subgroup of them, including *GADD45*α, *SLIT2*, *BAG1*, and *ATF4/CREB-2* but not *MAP3K14* (47). To further evaluate the consequences of NMD inhibition by Tax, we analyzed the half-lives of these five endogenous mRNAs in JPX9 cells with or without Tax induction. Cells were harvested at 0 h, 1.5 h, and 4 h after the addition of DRB, and these mRNAs were quantified by qRT-PCR, while Tax levels were monitored by immunoblotting (Fig. 8F). Interestingly, the *GADD45*α, *SLIT2*, and *ATF4/CREB-2*

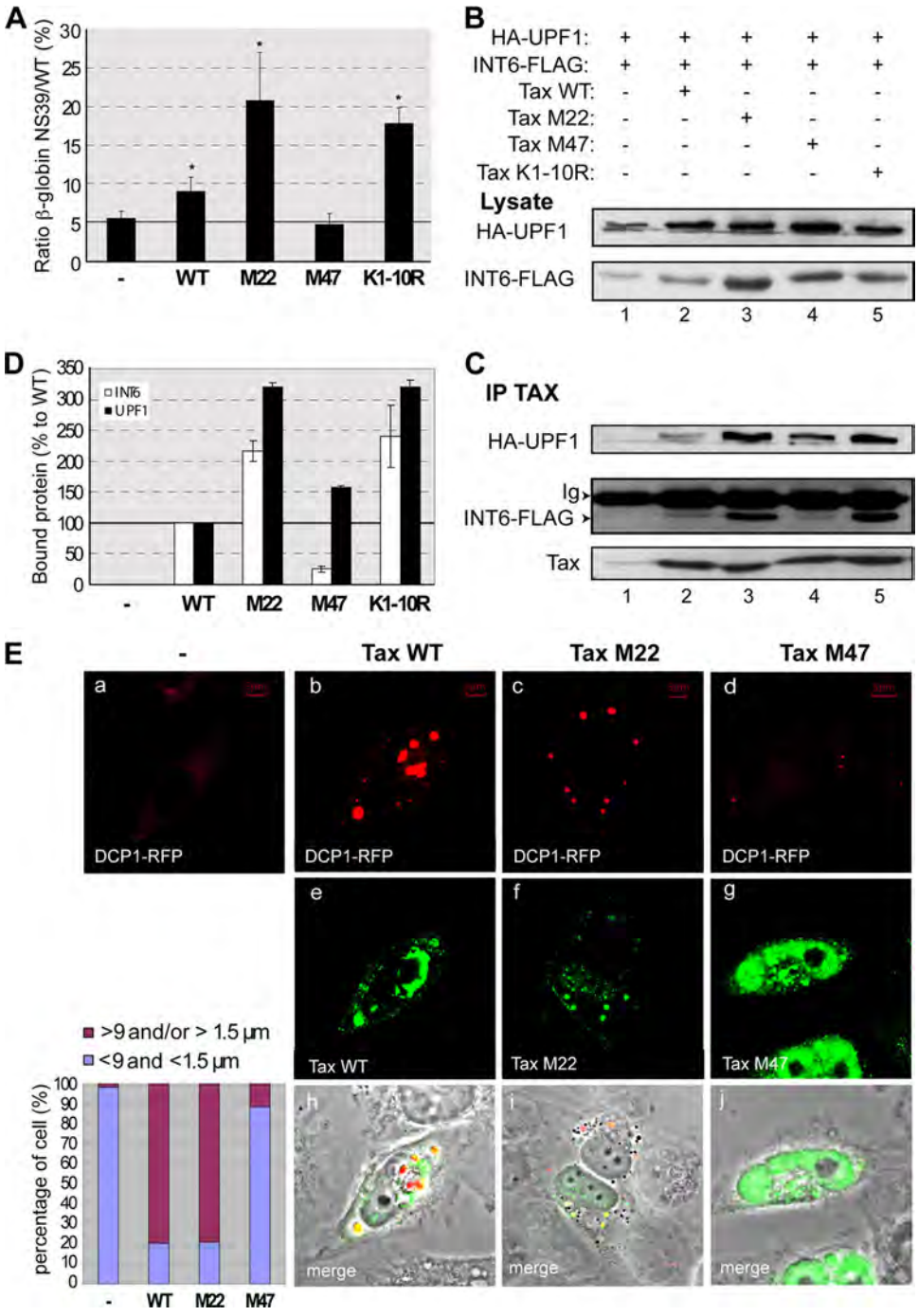

FIG 6 Tax mutants affect NMD efficiencies differently. (A) NMD assays were carried out, as described in the legend of Fig. 1A, with the cotransfection of control (−), wild-type (WT) Tax, Tax M22, Tax M47, and Tax K1-10R expression vectors (*, $P < 0.05$ [Student's t test P values refer to the control point {−}]). (B) Cells were transfected with the HA-UPF1, INT6-FLAG, and Tax expression vectors, as indicated. Extracts from these cells were analyzed by immunoblotting with antibodies to HA (top) and to FLAG (bottom). (C) Extracts from panel B were immunoprecipitated by using an antibody to Tax, and immunoprecipitates were analyzed with antibodies to HA (top), FLAG (middle), and Tax (bottom). Ig marks the immunoglobulin heavy chain. (D) Signals corresponding to HA-UPF1 and to INT6-FLAG in the immunoprecipitates from panel C were quantified and normalized to the signals detected in the extracts. The mean values obtained from three experiments are represented in a bar graph, with error bars corresponding to standard deviations. (E) Confocal microscopy analysis of HeLa cells transfected with constructs expressing DCP1-RFP together with a control (a) or vectors expressing either WT Tax (b and e), Tax M22 (c and f), or Tax M47 (d and g). The fluorescence from DCP1-RFP (red) and Tax immunostaining (green) is shown. The proportions of normal P-bodies ($n < 9$ and a diameter of <1.5 µm) and unusual P-bodies ($n > 9$ and/or a diameter of >1.5 µm) are presented in a bar graph.

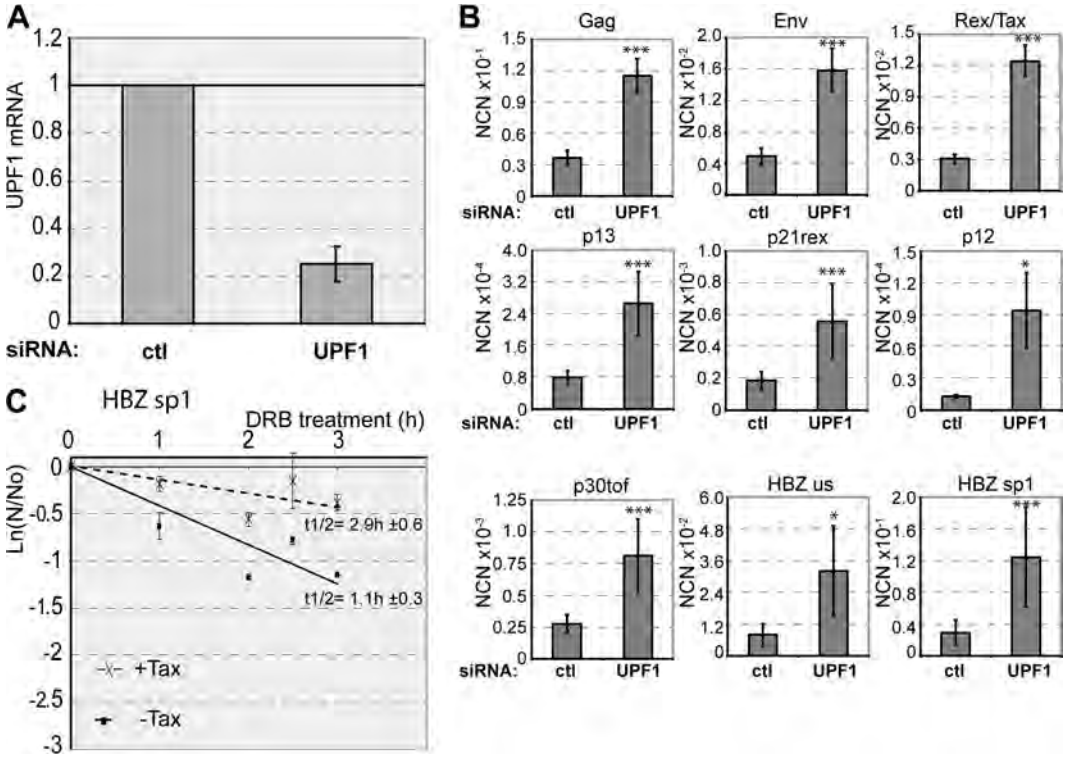

FIG 7 HTLV-1 mRNAs are sensitive to NMD. (A) HeLa cells were transfected first with 20 pmol of a control or UPF1 siRNA and 48 h later with the HTLV-1 molecular clone construct pACH. UPF1 mRNA from these cells was quantified to control the silencing efficiency. (B) Using these cells, the normalized copy number (NCN) of the various HTLV-1 transcripts in control and UPF1-silenced cells was determined by qRT-PCR. The mean values obtained from six experimental points are presented in the bar graphs for each viral transcript, with error bars corresponding to standard deviations. The results of Student's *t* tests are also indicated (*, $P < 0.05$; ***, $P < 0.001$). (C) The half-life of the *HBZ sp1* mRNA was measured in HeLa cells transfected with or without Tax. The amounts of *HBZ* mRNA were measured by qRT-PCR at each time point after the addition of DRB and normalized to *Renilla* mRNA levels, and the natural logarithm of the values, expressed as fractions to time zero, were plotted against time.

mRNA half-lives were significantly increased in the presence of Tax (3.4-, 4.1-, and 3.9-fold, respectively). The *BAG1* mRNA half-life increased 1.9-fold (Fig. 8A to D). This was not the case for the *MAP3K14* mRNA (Fig. 8E). These observations confirmed that by acting on INT6, Tax is also able to increase the stability of various cellular NMD-sensitive mRNAs.

DISCUSSION

By analyzing the inhibitory effect of HTLV-1 factors on the NMD pathway, our results point to an important action of Tax through interactions with the INT6 and UPF1 cellular proteins. Our observations also add evidence for an important role of INT6 in mRNA degradation by the NMD pathway. While UPF1 inhibits translation by associating with eIF3 (31), our data suggest that INT6 participates in this eIF3-UPF1 complex. An issue which will require further evaluation is the dynamics of the process. Indeed, some considerations indicate that INT6 might be present at early as well as at late steps of the processing of an mRNA targeted for degradation (4, 47, 67). Interestingly, it was reported previously that a fraction of INT6 was associated with chromatin (8), and purification experiments have shown its presence in the RNA Pol II holoenzyme (P. Jalinot and J.-M. Egly, unpublished data). Together with our previous characterization of an interaction of INT6 with the CBP80 subunit of the cap binding complex (47), these observations indicate that INT6 might be loaded onto mRNA at an early step of its processing. Once the pioneer round of translation is completed, the mRNP is reconfigured (39) and routed toward active translation, with the presence of INT6 in the eIF3 complex then being necessary or not (26, 67). Alternatively, when the mRNA includes a PTC or another feature favoring NMD, UPF1 is phosphorylated, inhibits translation through interactions with eIF3, and triggers mRNA degradation (31, 40). The presence of INT6 in P-bodies, which concentrate NMD factors and degradative enzymatic activities, indicates that this protein is likely to stick to the mRNP until its degradation, as UPF1 does. This is not the case for other eIF3 subunits (26), which are likely removed at an earlier step.

The HTLV-1 Tax protein has been described as a potent transactivator of provirus expression but also as an immortalizing protein with pleiotropic activities. In this report, we show a novel effect of Tax: the inhibition of the NMD pathway. We observed that Tax binds both INT6 and UPF1 but inhibits the presence of both proteins in the same complex. The analysis of Tax mutants indicated that the Tax-INT6 association is necessary for NMD inhibition, and our data suggest that Tax sequesters INT6 out of reach from UPF1. Tax also binds to UPF1 and causes an increase in the amount of phospho-UPF1. These activities coincide with an enhanced localization of UPF1 in the P-bodies, in which Tax was also partially detected. Tax-expressing cells also showed an increase in the number and size of the P-bodies. In agreement with previous studies performed in particular with a chemical inhibitor of NMD (17), this effect is likely due to the inhibition of mRNA

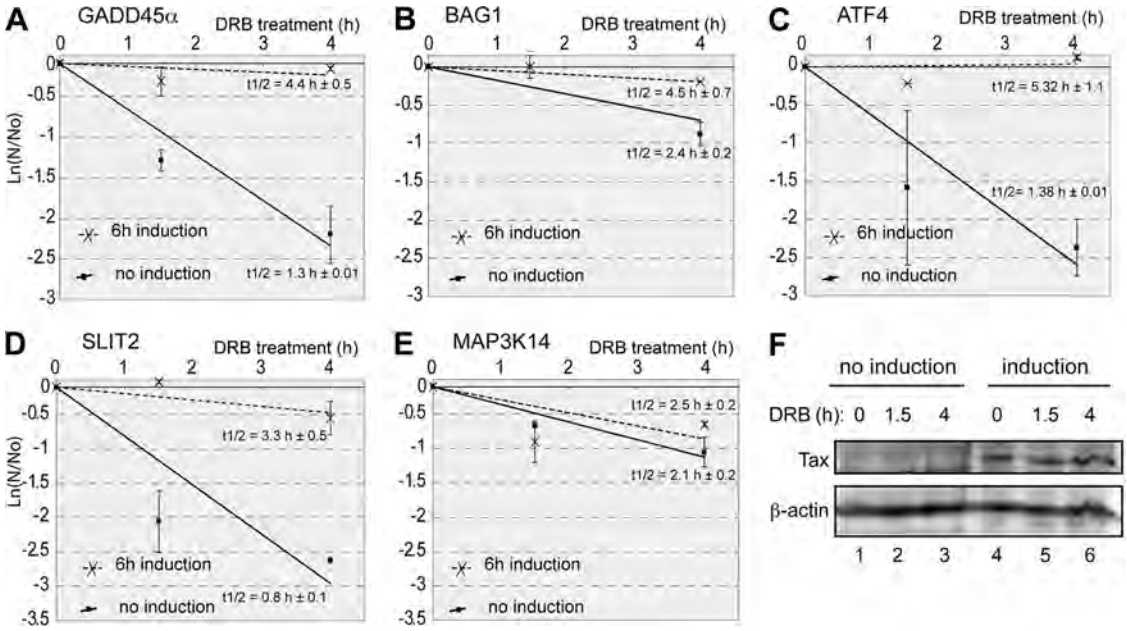

FIG 8 (A) The half-life of the *GADD45*α mRNA was measured in noninduced (squares and full line) and 6-h-induced (crosses and dotted line) JPX9 cells. The amounts of *GADD45*α mRNA were measured by qRT-PCR at each time point after the addition of DRB and normalized to GAPDH mRNA levels, and the natural logarithms of the values, expressed as fractions to time zero, were plotted against time. Each point corresponds to the mean of data from three independent measurements, and error bars indicate standard deviations. The half-life of the mRNA under both conditions was calculated and is indicated in the graph. (B to E) Same as in panel A but for *BAG1* (B), *ATF4/CREB-2* (C), *SLIT2* (D), and *MAP3K14* mRNAs (E). (F) Zero hours, 1.5 h, and 4 h after the addition of DRB, extracts of noninduced (lanes 1 to 3) or 6-h-induced (lanes 4 to 6) JPX9 cells were prepared and analyzed by immunoblotting using antibodies to Tax (top) and to β-actin (bottom).

degradation. The colocalization of Tax within the P-bodies revealed a new cytoplasmic localization of this viral protein. Interestingly, the modification by Tax of other cytoplasmic granules known to be involved in mRNA processing was recently documented (38). Moreover, through the SMG5 and SMG7 proteins, UPF1 was shown to be dephosphorylated by PP2A, thereby allowing its recycling (41). Knowing that Tax is able to maintain IKKγ in an active state by inhibiting its dephosphorylation by PP2A (22, 29), it is likely that Tax impedes the dephosphorylation of UPF1 by inhibiting this phosphatase in a similar manner. As a consequence, the Tax-UPF1 complexes would accumulate in the P-bodies, preventing the recycling of this core NMD factor and thereby interfering with complete mRNA degradation and inhibiting NMD (21) (Fig. 9).

It was recently reported that the inhibition of NMD is an important part of the development of tumorigenesis (63). Moreover, approximately 30% of cancers are considered to result from premature stop codons in tumor suppressor genes, which then escape NMD and lead to truncated dominant negative mutants. The Tax-dependent NMD inhibition that we observed might extend such an effect to an in-frame PTC due to mutations or alternative splicing events, which frequently occur in T cells (42). Considering our observation that NMD is globally downregulated in HTLV-1 cells expressing Tax, it can be speculated that this inhibition plays a role in the transformation of infected cells. Here, we limited our analysis of the impact of Tax on cellular mRNAs to those previously described to be stabilized after the silencing of UPF1, UPF2, or INT6 (45, 47, 65). Among these cellular genes, ATF4/CREB-2, for instance, which is regulated by NMD due to the presence of three uORFs (25), plays a role in HTLV-1 pathogenicity by heterodimerizing with AP-1 family transcription factors and has been associated with T-cell transformation through AP-1-responsive genes (23). Moreover, with the knowledge that modifications in RNA stability are an important source of gene expression alterations in stressed cells (20), future systematic studies of NMD-sensitive transcripts increased by Tax should help to define more precisely how this activity of Tax contributes to cell transformation. Among the viral genes, the expression of the antisense gene *HBZ* is clearly detectable throughout infection at the RNA level (56, 59). The current hypothesis is that the *HBZ* gene has a dual functionality: the *HBZ* mRNA promotes T-cell proliferation (55), while the HBZ protein suppresses Tax-mediated viral transcription (41). In line with its sensitivity to UPF1-mediated degradation, our data show that Tax significantly stabilizes *HBZ* mRNA. This observation illustrates the complexity of the cross talk between both viral proteins. By affecting both cellular and *HBZ* mRNAs, this inhibition of NMD by Tax is likely to contribute to cell transformation and the emergence of a leukemic clone of T lymphocytes. The inhibition of NMD can also be considered a potent means to significantly facilitate the expression of the HTLV-1 genome. In particular, ATF4/CREB-2 was reported previously to be involved in HTLV-1 LTR transactivation (24). This effect of Tax might then participate in the transcriptional induction of HTLV-1 provirus, since the increase of ATF4/CREB-2 protein levels by NMD inhibition is a well-described effect (25). Our data also show that some HTLV-1 mRNAs are sensitive to UPF1-mediated degradation. This suggests that viral mRNA expression downstream of activated transcription is also regulated at the posttranscriptional level. Thus, it is likely that in addition to its important effect on transcription, Tax would also intervene by

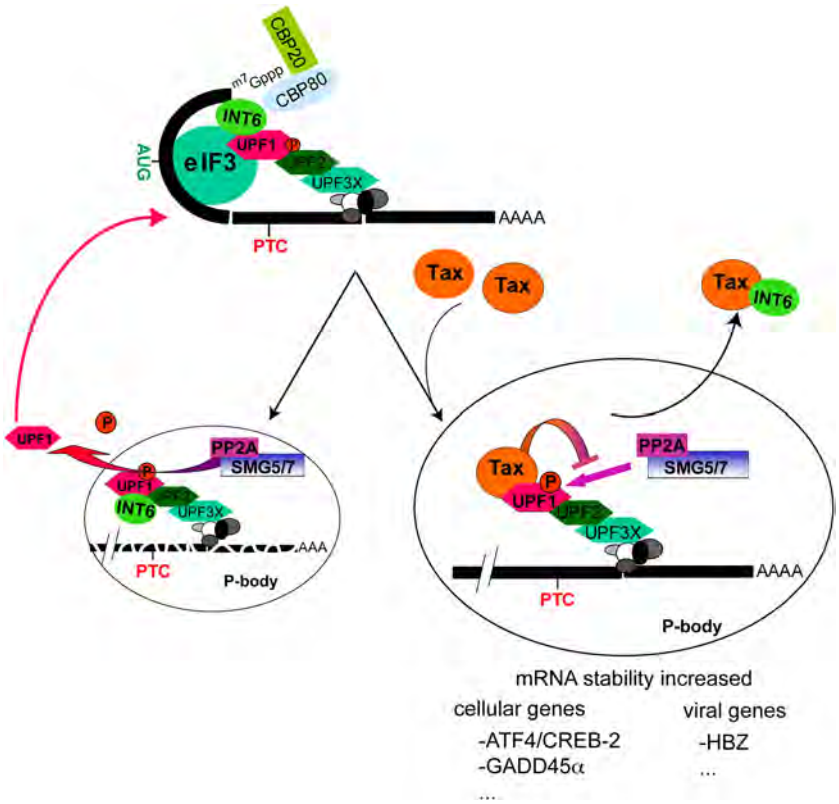

FIG 9 Summary scheme of the effect of Tax on the NMD pathway. In the case of an NMD-prone mRNA, UPF1 is phosphorylated by the SMG1 kinase and associates with UPF2 and UPF3. Under these conditions, UPF1 represses translation initiation by interacting with eIF3. Phosphorylated UPF1 also triggers an association with mRNA decay factors such as DCP1, XRN1, and the exosome component EXOSC2. After mRNA routing toward P-bodies, it is considered that UPF1 is dephosphorylated by the SMG5/7-PP2A complex and recycled (left bottom part of the scheme). In Tax-expressing cells, from the data presented in this report, Tax binds INT6, thereby impairing the INT6-UPF1 association. Tax also binds phospho-UPF1 and presumably prevents its normal dephosphorylation by PP2A, thus causing an accumulation of phospho-UPF1 in the P-bodies (right bottom part of the scheme). These combined effects lead to the stabilization of cellular as well as viral mRNAs by inhibiting their degradation.

allowing the escape of the RNAs from degradation. While NMD could be an effective protective mechanism against viral infection, Tax allows an escape from it, favoring the expression and persistence of the virus.

In conclusion, although NMD has already been associated with host-pathogen biology (2, 37), we report here for the first time that an HTLV-1 regulatory protein actively interferes with this pathway. While our observations establish that Tax is a major player in this inhibition, other viral proteins might also play a role. In this regard, it is worth mention that the NMD inhibition observed in HTLV-1-infected cell lines such as HUT102 was more potent than that observed in HeLa or Jurkat cells by expressing Tax alone. Whatever the contribution of other viral factors, our results show that Tax not only controls the transcription of viral and cellular genes but also acts on the posttranscriptional outcome of the corresponding mRNAs. Thus, it will be important in the future to consider this NMD effect to reach a complete understanding of the oncogenic effects of HTLV-1.

ACKNOWLEDGMENTS

We are grateful to L. Gazzolo and F. Mortreux for critical reading of the manuscript; A. Yamashita, S. Ohno, and H.-M. Jäck for providing us with antibodies; and N. Kedersha, A. Kulozik, C. Sun, and J. Cate for plasmids. We also thank A. Roisin for help with cell culture and C. Lionnet and F. Simian-Lermé for their assistance with microscopes.

This work was supported by a fellowship (V.M.) and a grant from the Association pour la Recherche sur le Cancer and by a fellowship (J.N.) from the Ligue Nationale contre le Cancer.

REFERENCES

1. **Abbas S, Erpelinck-Verschueren CA, Goudswaard CS, Lowenberg B, Valk PJ.** 2010. Mutant Wilms' tumor 1 (WT1) mRNA with premature termination codons in acute myeloid leukemia (AML) is sensitive to nonsense-mediated RNA decay (NMD). Leukemia **24**:660–663.
2. **Amor S, et al.** 2010. Alternative splicing and nonsense-mediated decay regulate telomerase reverse transcriptase (TERT) expression during virus-induced lymphomagenesis in vivo. BMC Cancer **10**:571. doi:10.1186/1471-2407-10-571.
3. **Anczukow O, et al.** 2008. Does the nonsense-mediated mRNA decay mechanism prevent the synthesis of truncated BRCA1, CHK2, and p53 proteins? Hum. Mutat. **29**:65–73.
4. **Asano K, Phan L, Anderson J, Hinnebusch AG.** 1998. Complex formation by all five homologues of mammalian translation initiation factor 3 subunits from yeast Saccharomyces cerevisiae. J. Biol. Chem. **273**:18573–18585.
5. **Barbier J, et al.** 2007. Regulation of H-ras splice variant expression by cross talk between the p53 and nonsense-mediated mRNA decay pathways. Mol. Cell. Biol. **27**:7315–7333.
6. **Boelz S, Neu-Yilik G, Gehring NH, Hentze MW, Kulozik AE.** 2006. A chemiluminescence-based reporter system to monitor nonsense-mediated mRNA decay. Biochem. Biophys. Res. Commun. **349**:186–191.
7. **Boxus M, et al.** 2008. The HTLV-1 Tax interactome. Retrovirology **5**:76. doi:10.1186/1742-4690-5-76.
8. **Buchsbaum S, Morris C, Bochard V, Jalinot P.** 2007. Human INT6

interacts with MCM7 and regulates its stability during S phase of the cell cycle. Oncogene **26**:5132–5144.
9. **Caron C, et al.** 1993. Functional and biochemical interaction of the HTLV-I Tax1 transactivator with TBP. EMBO J. **12**:4269–4278.
10. **Cavanagh MH, et al.** 2006. HTLV-I antisense transcripts initiating in the 3′LTR are alternatively spliced and polyadenylated. Retrovirology **3**:15. doi:10.1186/1742-4690-3-15.
11. **Chamieh H, Ballut L, Bonneau F, Le Hir H.** 2008. NMD factors UPF2 and UPF3 bridge UPF1 to the exon junction complex and stimulate its RNA helicase activity. Nat. Struct. Mol. Biol. **15**:85–93.
12. **Chang YF, Imam JS, Wilkinson MF.** 2007. The nonsense-mediated decay RNA surveillance pathway. Annu. Rev. Biochem. **76**:51–74.
13. **Chiari E, et al.** 2004. Stable ubiquitination of human T-cell leukemia virus type 1 tax is required for proteasome binding. J. Virol. **78**:11823–11832.
14. **Couttet P, Grange T.** 2004. Premature termination codons enhance mRNA decapping in human cells. Nucleic Acids Res. **32**:488–494.
15. **Derse D, Mikovits J, Polianova M, Felber BK, Ruscetti F.** 1995. Virions released from cells transfected with a molecular clone of human T-cell leukemia virus type I give rise to primary and secondary infections of T cells. J. Virol. **69**:1907–1912.
16. **Desbois C, Rousset R, Bantignies F, Jalinot P.** 1996. Exclusion of Int-6 from PML nuclear bodies by binding to the HTLV-I Tax oncoprotein. Science **273**:951–953.
17. **Durand S, et al.** 2007. Inhibition of nonsense-mediated mRNA decay (NMD) by a new chemical molecule reveals the dynamic of NMD factors in P-bodies. J. Cell Biol. **178**:1145–1160.
18. **El-Bchiri J, et al.** 2005. Differential nonsense mediated decay of mutated mRNAs in mismatch repair deficient colorectal cancers. Hum. Mol. Genet. **14**:2435–2442.
19. **Englert C, et al.** 1995. Truncated WT1 mutants alter the subnuclear localization of the wild-type protein. Proc. Natl. Acad. Sci. U. S. A. **92**: 11960–11964.
20. **Fan J, et al.** 2002. Global analysis of stress-regulated mRNA turnover by using cDNA arrays. Proc. Natl. Acad. Sci. U. S. A. **99**:10611–10616.
21. **Franks TM, Singh G, Lykke-Andersen J.** 2010. Upf1 ATPase-dependent mRNP disassembly is required for completion of nonsense-mediated mRNA decay. Cell **143**:938–950.
22. **Fu DX, Kuo YL, Liu BY, Jeang KT, Giam CZ.** 2003. Human T-lymphotropic virus type I tax activates I-kappa B kinase by inhibiting I-kappa B kinase-associated serine/threonine protein phosphatase 2A. J. Biol. Chem. **278**:1487–1493.
23. **Fujii M, et al.** 2000. Activation of oncogenic transcription factor AP-1 in T cells infected with human T cell leukemia virus type 1. AIDS Res. Hum. Retroviruses **16**:1603–1606.
24. **Gachon F, Devaux C, Mesnard JM.** 2002. Activation of HTLV-I transcription in the presence of Tax is independent of the acetylation of CREB-2 (ATF-4). Virology **299**:271–278.
25. **Gardner LB.** 2008. Hypoxic inhibition of nonsense-mediated RNA decay regulates gene expression and the integrated stress response. Mol. Cell. Biol. **28**:3729–3741.
26. **Grzmil M, et al.** 2010. An oncogenic role of eIF3e/INT6 in human breast cancer. Oncogene **29**:4080–4089.
27. **Guo J, Sen GC.** 2000. Characterization of the interaction between the interferon-induced protein P56 and the Int6 protein encoded by a locus of insertion of the mouse mammary tumor virus. J. Virol. **74**:1892–1899.
28. **Holbrook JA, Neu-Yilik G, Hentze MW, Kulozik AE.** 2004. Nonsense-mediated decay approaches the clinic. Nat. Genet. **36**:801–808.
29. **Hong S, et al.** 2007. Heptad repeats regulate protein phosphatase 2a recruitment to I-kappaB kinase gamma/NF-kappaB essential modulator and are targeted by human T-lymphotropic virus type 1 tax. J. Biol. Chem. **282**:12119–12126.
30. **Ishigaki Y, Li X, Serin G, Maquat LE.** 2001. Evidence for a pioneer round of mRNA translation: mRNAs subject to nonsense-mediated decay in mammalian cells are bound by CBP80 and CBP20. Cell **106**:607–617.
31. **Isken O, et al.** 2008. Upf1 phosphorylation triggers translational repression during nonsense-mediated mRNA decay. Cell **133**:314–327.
32. **Jiang H, et al.** 1999. PCAF interacts with tax and stimulates tax transactivation in a histone acetyltransferase-independent manner. Mol. Cell. Biol. **19**:8136–8145.
33. **Kashima I, et al.** 2006. Binding of a novel SMG-1-Upf1-eRF1-eRF3 complex (SURF) to the exon junction complex triggers Upf1 phosphorylation and nonsense-mediated mRNA decay. Genes Dev. **20**:355–367.
34. **Kawasaki T, et al.** 1994. mRNA and protein expression of p53 mutations in human bladder cancer cell lines. Cancer Lett. **82**:113–121.
35. **Kedersha N, et al.** 2005. Stress granules and processing bodies are dynamically linked sites of mRNP remodeling. J. Cell Biol. **169**:871–884.
36. **King-Underwood L, Renshaw J, Pritchard-Jones K.** 1996. Mutations in the Wilms' tumor gene WT1 in leukemias. Blood **87**:2171–2179.
37. **LeBlanc JJ, Beemon KL.** 2004. Unspliced Rous sarcoma virus genomic RNAs are translated and subjected to nonsense-mediated mRNA decay before packaging. J. Virol. **78**:5139–5146.
38. **Legros S, et al.** 2011. The HTLV-1 Tax protein inhibits formation of stress granules by interacting with histone deacetylase 6. Oncogene **30**:4050–4062.
39. **Lejeune F, Ishigaki Y, Li X, Maquat LE.** 2002. The exon junction complex is detected on CBP80-bound but not eIF4E-bound mRNA in mammalian cells: dynamics of mRNP remodeling. EMBO J. **21**:3536–3545.
40. **Lejeune F, Li X, Maquat LE.** 2003. Nonsense-mediated mRNA decay in mammalian cells involves decapping, deadenylating, and exonucleolytic activities. Mol. Cell **12**:675–687.
41. **Lemasson I, et al.** 2007. Human T-cell leukemia virus type 1 (HTLV-1) bZIP protein interacts with the cellular transcription factor CREB to inhibit HTLV-1 transcription. J. Virol. **81**:1543–1553.
42. **Li S, Wilkinson MF.** 1998. Nonsense surveillance in lymphocytes? Immunity **8**:135–141.
43. **Matsuda D, Sato H, Maquat LE.** 2008. Studying nonsense-mediated mRNA decay in mammalian cells. Methods Enzymol. **449**:177–201.
44. **Matsuoka M, Jeang KT.** 2011. Human T-cell leukemia virus type 1 (HTLV-1) and leukemic transformation: viral infectivity, Tax, HBZ and therapy. Oncogene **30**:1379–1389.
45. **Mendell JT, Sharifi NA, Meyers JL, Martinez-Murillo F, Dietz HC.** 2004. Nonsense surveillance regulates expression of diverse classes of mammalian transcripts and mutes genomic noise. Nat. Genet. **36**:1073–1078.
46. **Morris C, Jalinot P.** 2005. Silencing of human Int-6 impairs mitosis progression and inhibits cyclin B-Cdk1 activation. Oncogene **24**:1203–1211.
47. **Morris C, Wittmann J, Jack HM, Jalinot P.** 2007. Human INT6/eIF3e is required for nonsense-mediated mRNA decay. EMBO Rep. **8**:596–602.
48. **Morris-Desbois C, Bochard V, Reynaud C, Jalinot P.** 1999. Interaction between the Ret finger protein and the Int-6 gene product and co-localisation into nuclear bodies. J. Cell Sci. **112**(Pt 19):3331–3342.
49. **Muhlemann O, Lykke-Andersen J.** 2010. How and where are nonsense mRNAs degraded in mammalian cells? RNA Biol. **7**:28–32.
50. **Nasr R, et al.** 2006. Tax ubiquitylation and sumoylation control critical cytoplasmic and nuclear steps of NF-kappaB activation. Blood **107**:4021–4029.
51. **Ohnishi T, et al.** 2003. Phosphorylation of hUPF1 induces formation of mRNA surveillance complexes containing hSMG-5 and hSMG-7. Mol. Cell **12**:1187–1200.
52. **Perrin-Vidoz L, Sinilnikova OM, Stoppa-Lyonnet D, Lenoir GM, Mazoyer S.** 2002. The nonsense-mediated mRNA decay pathway triggers degradation of most BRCA1 mRNAs bearing premature termination codons. Hum. Mol. Genet. **11**:2805–2814.
53. **Rehwinkel J, Behm-Ansmant I, Gatfield D, Izaurralde E.** 2005. A crucial role for GW182 and the DCP1:DCP2 decapping complex in miRNA-mediated gene silencing. RNA **11**:1640–1647.
54. **Rende F, et al.** 2011. Kinetics and intracellular compartmentalization of HTLV-1 gene expression: nuclear retention of HBZ mRNAs. Blood **117**: 4855–4859.
55. **Satou Y, Matsuoka M.** 2007. Implication of the HTLV-I bZIP factor gene in the leukemogenesis of adult T-cell leukemia. Int. J. Hematol. **86**:107–112.
56. **Satou Y, Yasunaga J, Yoshida M, Matsuoka M.** 2006. HTLV-I basic leucine zipper factor gene mRNA supports proliferation of adult T cell leukemia cells. Proc. Natl. Acad. Sci. U. S. A. **103**:720–725.
57. **Sheth U, Parker R.** 2006. Targeting of aberrant mRNAs to cytoplasmic processing bodies. Cell **125**:1095–1109.
58. **Smith MR, Greene WC.** 1990. Identification of HTLV-I tax trans-activator mutants exhibiting novel transcriptional phenotypes. Genes Dev. **4**:1875–1885.
59. **Suemori K, et al.** 2009. HBZ is an immunogenic protein, but not a target antigen for human T-cell leukemia virus type 1-specific cytotoxic T lymphocytes. J. Gen. Virol. **90**:1806–1811.
60. **Sun C, et al.** 2011. Functional reconstitution of human eukaryotic trans-

lation initiation factor 3 (eIF3). Proc. Natl. Acad. Sci. U. S. A. **108**:20473–20478.
61. **Tatewaki M, et al.** 1995. Constitutive overexpression of the L-selectin gene in fresh leukemic cells of adult T-cell leukemia that can be transactivated by human T-cell lymphotropic virus type 1 Tax. Blood **86**:3109–3117.
62. **Terme JM, et al.** 2008. Cross talk between expression of the human T-cell leukemia virus type 1 Tax transactivator and the oncogenic bHLH transcription factor TAL1. J. Virol. **82**:7913–7922.
63. **Wang D, et al.** 2011. Inhibition of nonsense-mediated RNA decay by the tumor microenvironment promotes tumorigenesis. Mol. Cell. Biol. **31**: 3670–3680.
64. **Watkins SJ, Norbury CJ.** 2004. Cell cycle-related variation in subcellular localization of eIF3e/INT6 in human fibroblasts. Cell Prolif. **37**:149–160.
65. **Wittmann J, Hol EM, Jack HM.** 2006. hUPF2 silencing identifies physiologic substrates of mammalian nonsense-mediated mRNA decay. Mol. Cell. Biol. **26**:1272–1287.
66. **Yamashita A, et al.** 2009. SMG-8 and SMG-9, two novel subunits of the SMG-1 complex, regulate remodeling of the mRNA surveillance complex during nonsense-mediated mRNA decay. Genes Dev. **23**:1091–1105.
67. **Zhou C, et al.** 2005. PCI proteins eIF3e and eIF3m define distinct translation initiation factor 3 complexes. BMC Biol. **3**:14. doi:10.1186/1741-7007-3-14.

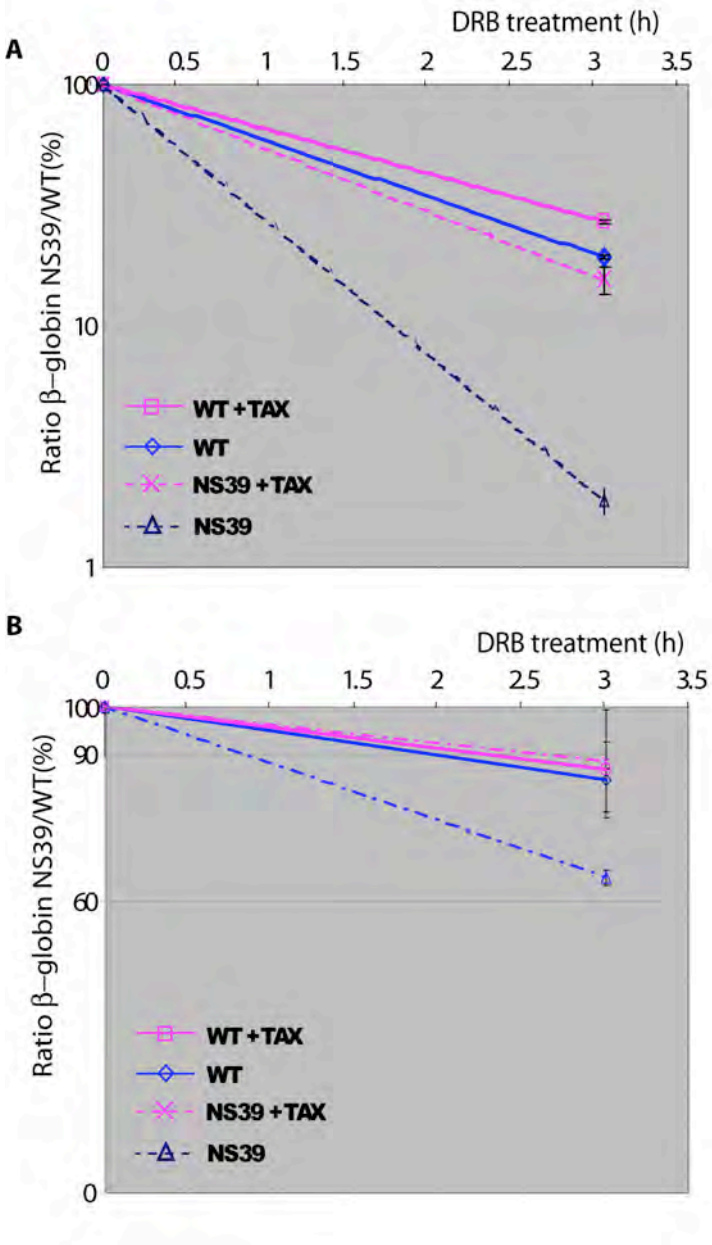

Supplemental Figure 1: Decay of the GlWT and GlNS39 mRNA in the absence and presence of Tax. A: NMD assay was carried out with JPX9 cells (see materials and methods) with 6h of Tax induction (square/full line or cross/dotted line, respectively) or without (diamond/full line or triangle/dotted line, respectively). Cells were treated or not with 100 µg/ml DRB for 3h. Renilla luciferase signal was measured and the luciferase mRNA decay was represented in a graph. It shows that Tax specifically stabilizes the premature stop codon containing mRNA as compared to the WT. **B**: HeLa cells were transfected with β-globin reporter plasmids (Gl WT, full line, or Gl NS39, dotted line) and a control (diamonds or triangles, respectively) or a Tax expression vector (squares or crosses, respectively). Cells were treated with or without 100 µg/ml DRB for 3h. Total mRNA was extracted and the globin mRNA was quantified by qRT-PCR and normalized to the *GAPDH* mRNA. The globin mRNA decay for each condition is represented in the graph and shows that Tax specifically stabilizes the Gl NS39 mRNA as compared to the Gl WT.

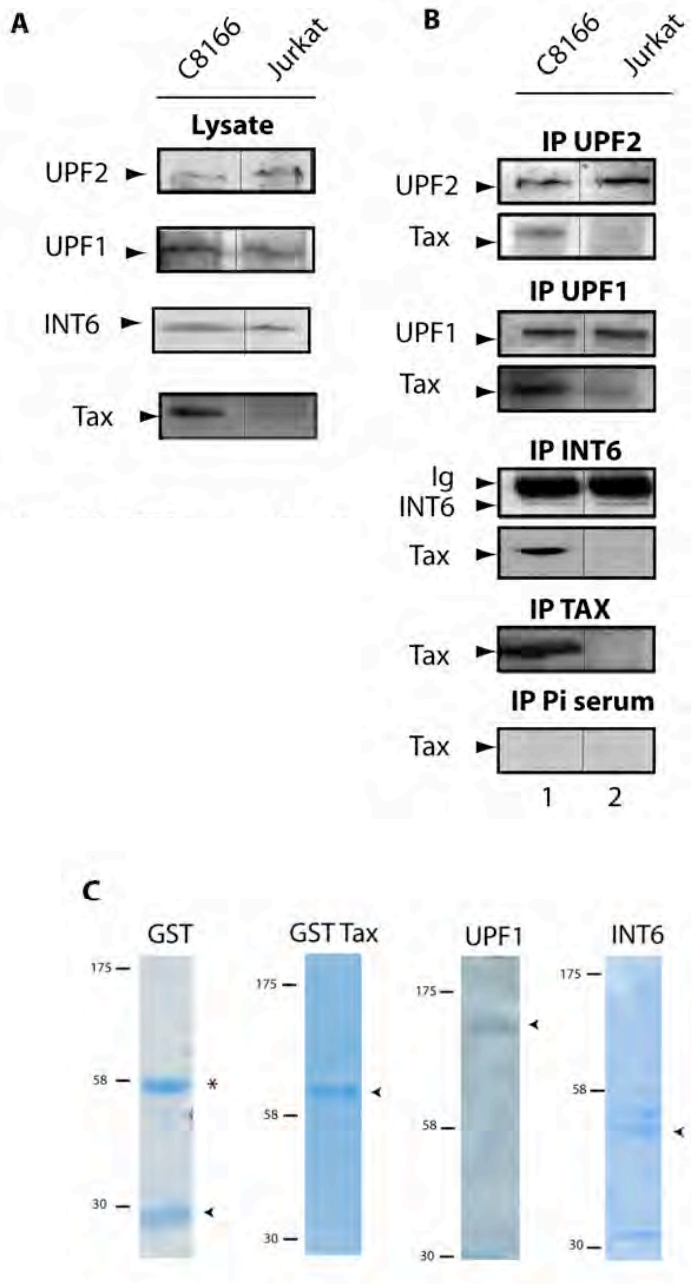

Supplemental Figure 2 : Tax binds NMD factors. A: Endogenous NMD factors from C8166 (lane 1) and Jurkat (lane 2) extracts treated with RNAse were analyzed by immunoblot using the following antibodies from the top panel to the bottom: UPF2, UPF1, INT6. Immunoblot analysis was also performed with an atibody to Tax. No significant difference is observed in NMD protein levels between these two cell lines. **B**: Immunoprecipitations using these extracts were carried out as indicated and the immunoprecipitates were analysed by immunoblot as in A for both the immunoprecipitated protein and Tax. Immunoprecipitation was also performed using preimmune serum as control. The lanes 1 and 2 were on the same blot, but separated by an additional unrelated lane which has been removed as indicated by the vertical line. **C**: GST, GST-TAX, INT6 and UPF1 were produced in bacteria and purified. Arrow heads indicate the position of the purified protein in Coomassie Blue-stained gels (* indicates the GST dimer).

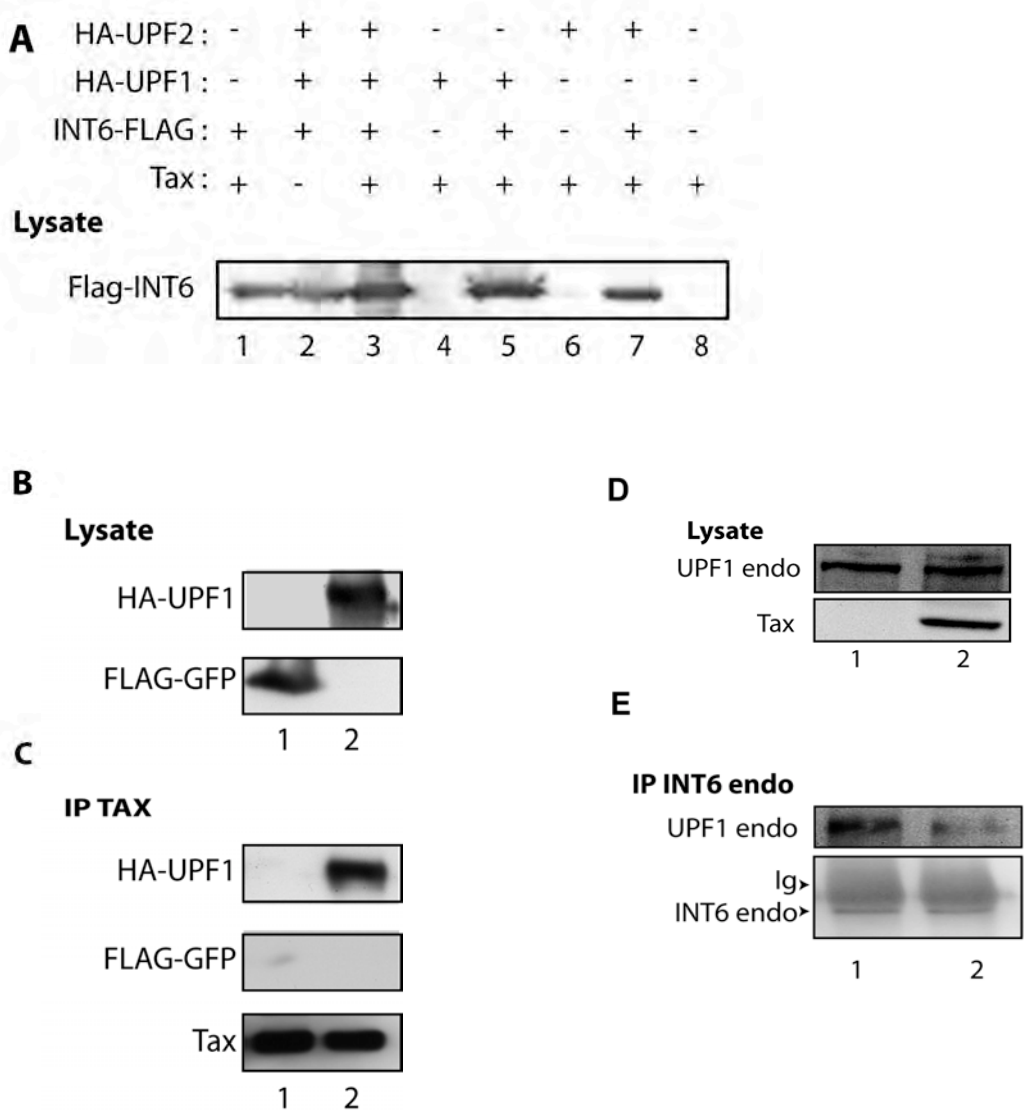

Supplemental Figure 3 : Tax inhibits UPF1 and INT6 association *in vitro*. A: Tax, INT6-FLAG, HA-UPF1 and HA-UPF2 expression vectors were transfected in 293T cells as indicated in Figure 2A. The expression of INT6-FLAG was analysed by immunoblot using antibodies to FLAG. There was not significant change in the levels of INT6. **B**: Tax and FLAG-GFP (lane 1) or Tax and HA-UPF1 (lane 2) expression vectors were transfected in 293T cells; the expression of HA-UPF1 and FLAG-GFP was assessed by immunoblot using extracts of these cells. **C**: these extracts were used to carry out immunoprecipitation using an antibody to Tax. The absence of FLAG-GFP in lane 1 confirms the specificity of the Tax/UPF1 association in lane 2. **D:** HeLa cells were transfected with a control (lane 1) or a Tax (lane 2) expression vector. Levels of endogenous UPF1 and Tax were analysed by immunoblot. **E**: Extracts from D were immunoprecipitated with an antibody to INT6 (N-19) and immunoprecipitates were analysed by immunoblot with antibodies to UPF1 (top panel) and to INT6 (bottom panel). The presence of Tax causes a decrease in the level of UPF1 associated to INT6.

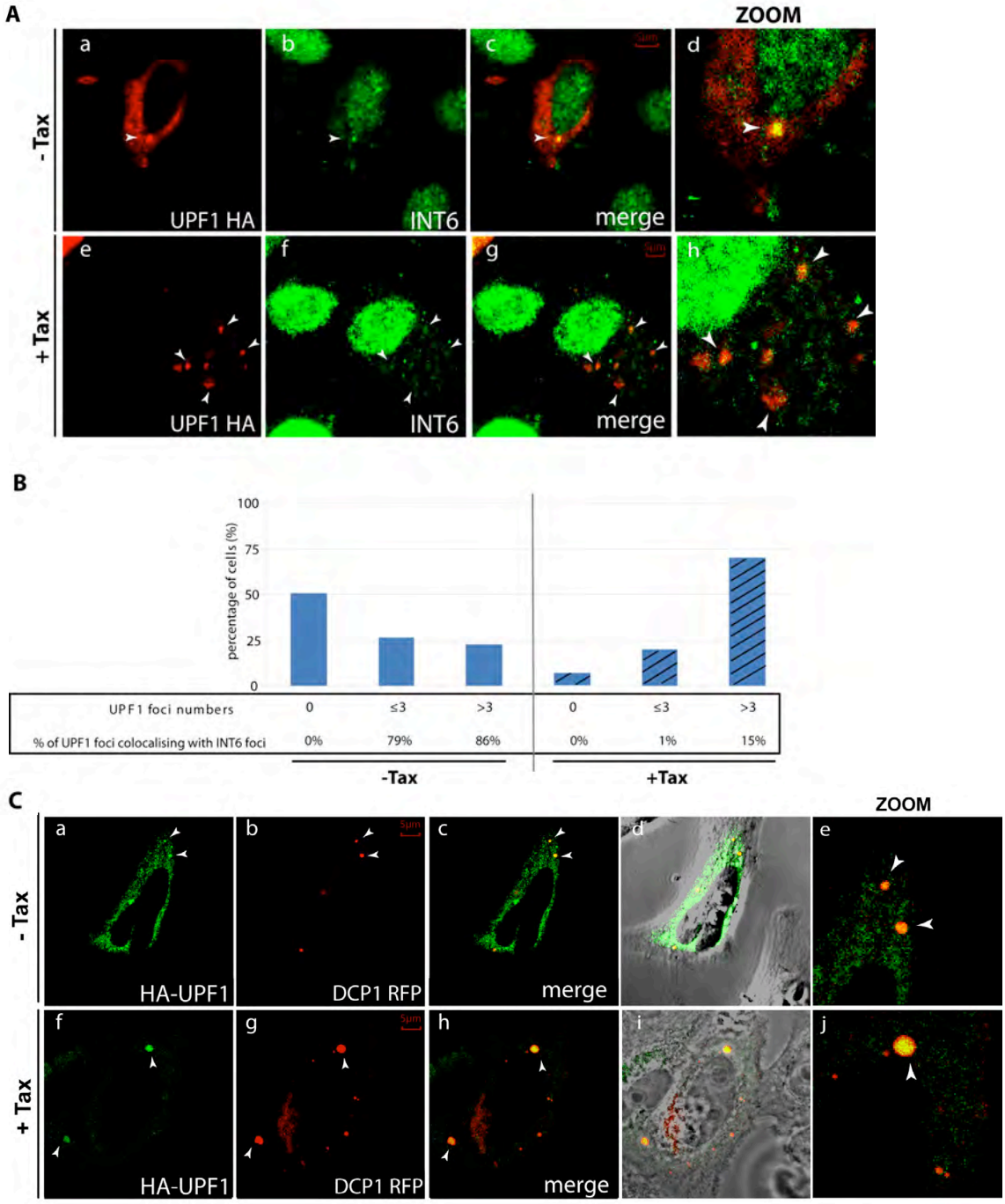

Supplemental Figure 4 : Tax inhibits UPF1 and INT6 association. A: Confocal microscopy analysis of HeLa cells transfected with HA-UPF1 and with a control (panels a-d) or Tax expression vectors (panels e-h). Immunostaining was done with an antibody to HA (panels a, e) and to INT6 (panels b,f). Superposition of both stainings is shown in panels c and g. **B**: UPF1 foci were quantified (0, ≤3, >3) in several cells in the absence or presence or Tax. Results are indicated below bars corresponding to the percentage of cells. Colocalization of HA-UPF1 and INT6 in these foci was also analysed. These data show that the presence of Tax increases the number of UPF1 foci, but decreases the presence of INT6 in these foci. **C**: Confocal microscopy analysis of HeLa cells transfected with HA-UPF1 and DCP1-RFP expression vectors together with a control (panels a-e) or Tax (panels f-j) expression vector. Immunostaining was done with an antibody to HA and appears in green (panels a, f). The DCP1-RFP red fluorescence was analyzed and is represented alone (panels b, g) or with the HA fluorescence (panels c and h). Panels d and i show the transmission image and panels e and j are an enlargement of P-bodies examples indicated by arrows.

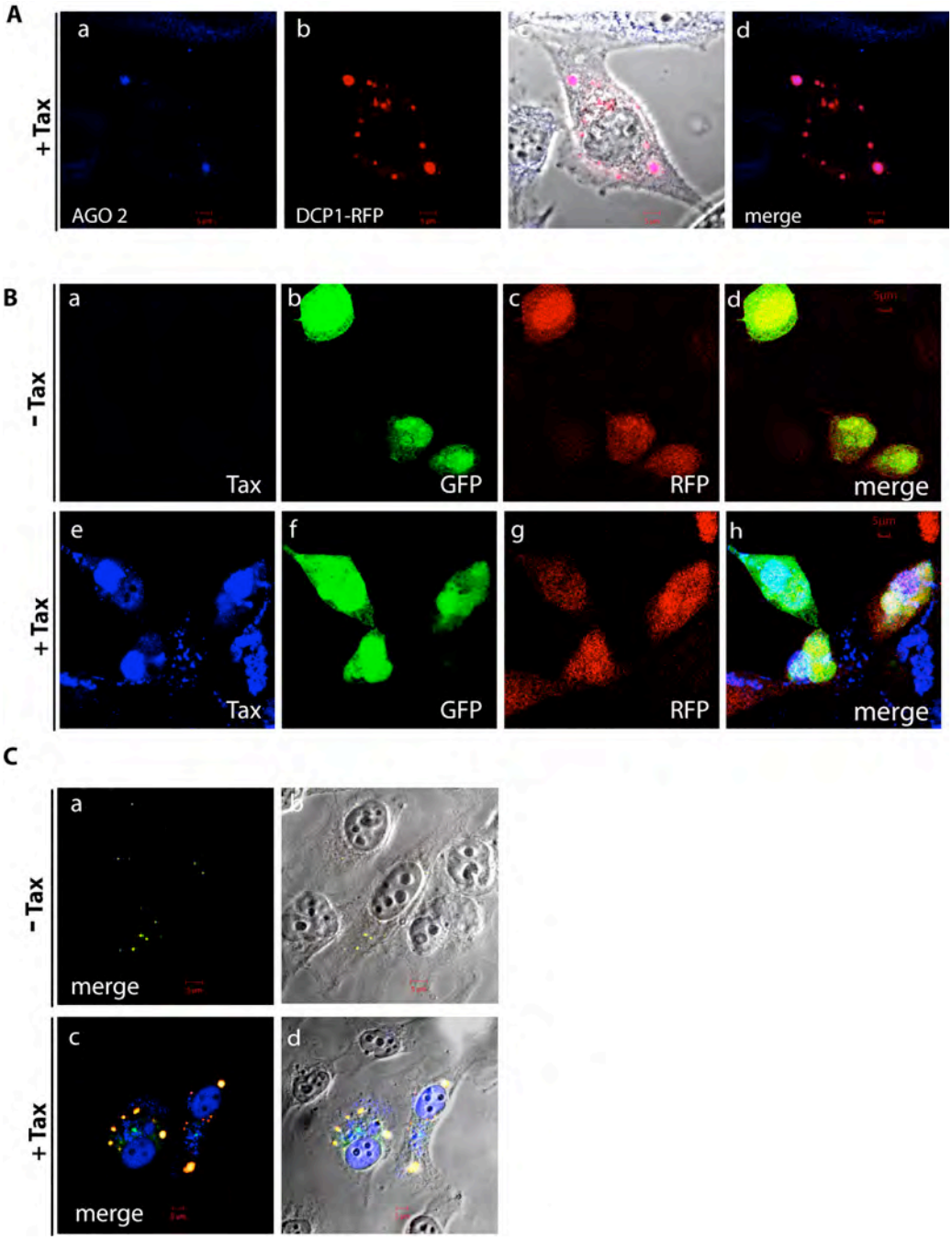

Supplemental Figure 5 : P-bodies are modified in the presence of Tax. **A** : HeLa cells were transfected with Tax and DCP1-RFP expression vectors. Immunostaining with an antibody directed against endogenous AGO2 (blue, panel a), as observed by confocal microscopy is shown for a representative cell, along with red fluorescence of DCP1-RFP (panel b). Superposition of both stainings with (panel c) or without transmission image (panel d) are shown. These pictures confirm the effect of Tax on P-bodies with an endogenous component of these structures. **B**: HeLa cells were transfected with expression vectors for GFP and RFP. Control (pSG5; panel a-d) or Tax (panels e-h) expressing plasmids were also transfected. Immunostaining with antibody to Tax (blue, panels a, e) along with GFP green fluorescence (panels b, f) and RFP red fluorescence (panels c, g) as observed by confocal microscopy are shown for representative cells. Superposition of all three stainings is also shown (panels d, h). This control shows that Tax by itself does not affect subcellular localization of the GFP and RFP proteins. **C** : Merge and transmission view of the confocal pictures from Figure 4D.

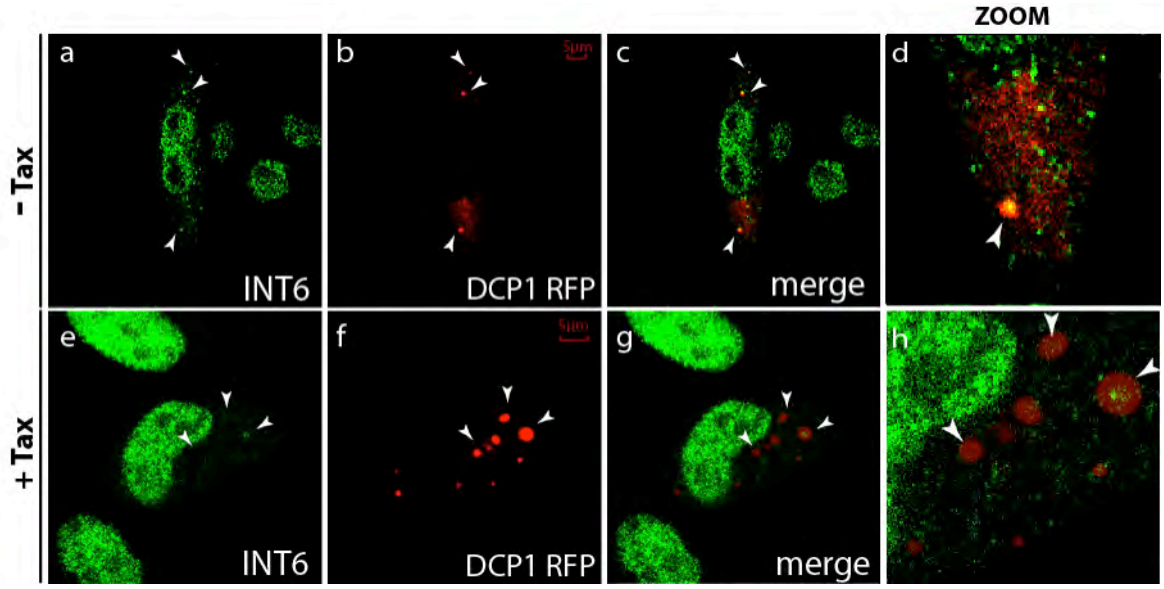

Supplemental Figure 6 : INT6 is delocalized from the P-bodies in the presence of Tax. HeLa cells were transfected with the DCP1-RFP expression vector, together with control (pSG5, panels a-d) or Tax (panels e-h) expression vectors. Cells were treated and depicted as described for supplemental figure 4C except that immunostaining was carried out using an antibody directed against INT6 (C-169) (panels a, e). Here we observed that to the opposite of UPF1, INT6 is less present in the P-bodies in the presence of Tax. This corroborates a dissociation between INT6 and UPF1 in the presence of Tax.

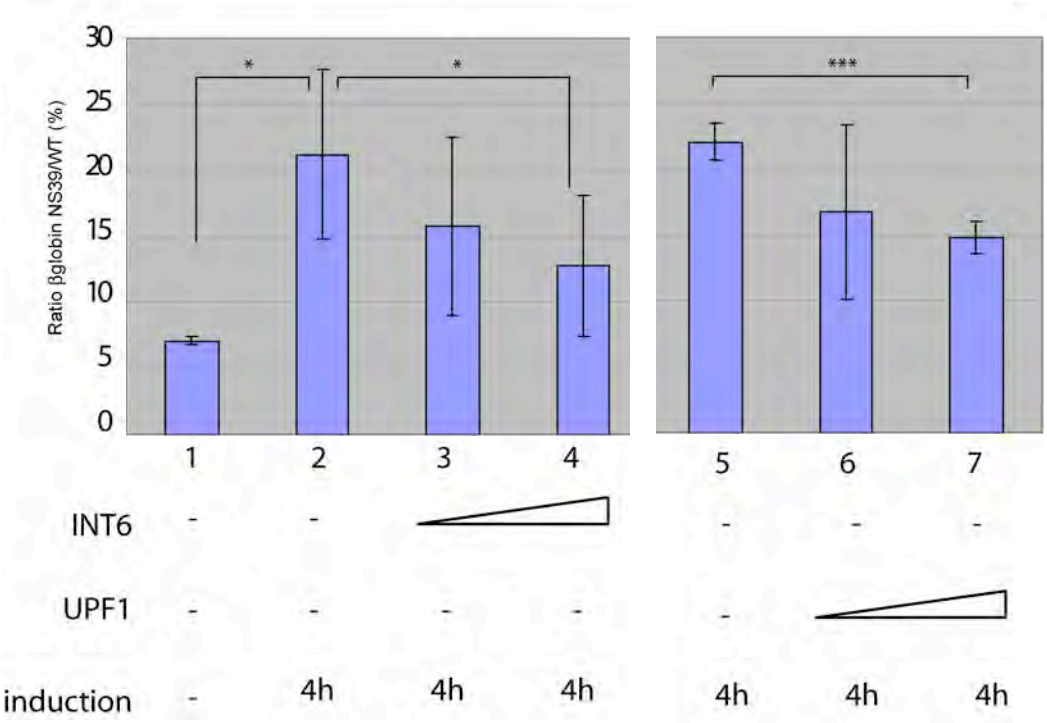

Supplemental Figure 7: INT6 as well as UPF1 overexpression reverses NMD inhibition by Tax. NMD assays were performed using induced JPX9 cells as described in Figure 1C, except that an increasing amount of INT6 expression vector (0.7 µg and 2 µg) or UPF1 (3 µg and 6 µg) was co-transfected with the renilla luciferase/globin plasmids. (*P<0.05 ; ***P<0.005). These data show that the overexpression of INT6 is able to decrease by 39% the NMD inhibition despite the presence of Tax, demonstrating the competitive relationship between Tax and INT6 in the process. The decrease by 23% of the NMD inhibition after the overexpression of UPF1 also confirms the importance of the Tax/UPF1 association in the process.